IRF2BP2, a Novel Transcriptional Regulator of Innate Immunity, Cholesterol Metabolism and Atherosclerosis

Dr. Kianoosh Keyhanian

Master's candidate
Neuroscience program
University of Ottawa

Under supervision of:

Dr. Hsiao-Huei Chen
Dr. Alexandre F.R Stewart

© Kianoosh Keyhanian, Ottawa, Canada, 2014

Table of Contents

Acknowledgments

It was a great privilege for me to be a student at Dr. Hsiao-Huei Chen's laboratory. I deeply appreciate her kind support and persistent motivations. It was also an honor to receive support and scientific guidance from Dr. Alexandre F.R. Stewart as my co-supervisor. Their genuine enthusiasm in science was very inspiring for me, and their encouragements helped me learn and thrive all through my project.

I cannot thank the lab members enough. Special thanks to Xun Zhou who patiently taught me the initial steps in the laboratory and had helped me remarkably in my project; to Dr. Nihar Pandey for his continuous support as well as his significant contributions in the project; and to Tiffany Ho who generously helped me with my cholesterol measuring and atherosclerosis experiments. I also appreciate Dr. Zhaohong Qin and Dr. Tariq Zaman for their help and supports. I am very grateful for Dr. Katey Rainer's kind collaboration in performing FPLC and bone marrow transplant experiments. I would like to thank my thesis advisory committee members, Dr. Wandong Zhang and Dr. Thomas Lagace, for their invaluable suggestions and comments. I also appreciate Dr. Zha and Dr. Sorisky and their lab members for providing us with protocols and guiding us through the macrophage metabolism experiments. I am also very grateful to Dr. David Grynspan from whom I learned a great deal about the histology of our mouse model.

Finally, I would like to express my deepest appreciation to my family. My husband's kindest support, faith, patience and love have been my greatest source of motivation. And my parents' love and prayers is what I am always blessed with.

Abbreviations

ABCA1, ABCG1: ATP-binding cassette transporter A1 or G1

AcLDL: Acetylated Low Density Lipoprotein

ApoE-/-: Transgenic mice deficient in apolipoprotein E

BMDM: Bone Marrow Derived Macrophages

CCL2: Chemokine (C-C motif) Ligand 2

CCL5: Chemokine (C-C motif) Ligand 5

CCL10: Chemokine (C-C motif) Ligand 10

CX3CL1: Chemokine (C-X3-C Motif) Ligand 1

DAPI, 4',6-diamidino-2-phenylindole

FPLC: Fast Protein Liquid Chromatography

GEMM-CFU: Granulocyte-Erythrocyte- Megakaryocyte-Macrophage Colony Forming Unit

GMM-CFU: Granulocyte-Monocyte Colony Forming Unit

GWAS: Genome Wide Association Study

GTT: Glucose Tolerance Test

HET: heterozygote for IRF2BP2 allele in myeloid lineage: LysMcre $IRF2BP2_{flx/wt}$

HFD: High Fat Diet

HDL: High Density Lipoprotein

IDL: Intermediate Density Lipoprotein

IL-1, IL-4: Interleukin-1, Interleukin-4

IRF2: Interferon Regulatory Factor 2

IRF2BP2: IRF2 Binding Protein 2

$IRF2BP2_{flx/flx}$: a transgenic mouse bearing loxP sites that flank the IRF2BP2 gene

IRF2BP2MKO: Specific ablation of IRF2BP2 in mice myeloid lineage (LysMcre/IRF2BP2$_{flx/flx}$) KO: Knock Out

LC: Littermate control

LOX1: Lectin-type oxidized LDL receptor 1, aka Oxidized LDL Receptor 1 (OLR1)

LXR: Liver X Receptor

LPS: Lipopolysaccharide

LysMcre: a transgenic mouse carrying the Cre recombinase inserted into the lysozyme2 gene

MCP1: monocyte chemotactic protein 1

M-CSF: Monocyte - Colony Stimulating Factor

NFAT1: Nuclear Factor of Activated T Cells 1

MKO→LDLR-/-: LDLR-/- mice that were transplanted with bone marrow from IRF2BP2MKO mice.

NR4A1: Nuclear Receptor 4A1

NLRP3: Nucleotide-binding domain and Leucine-rich Repeat family, Pyrin domain containing 3

OxLDL: oxidized Low Density Lipoprotein

PPARg, PPARd: Peroxisome Proliferator-Activated Receptor gamma, delta

RER: Respiratory Exchange Ratio

SCARA1, SCARB1: Scavenger receptor A1, B1

STAT1: Stimulator of Activated T-cells 1

TH1: T Helper 1 cell

TLR2: Toll-like Receptor 2

TLR4: Toll-like Receptor 4

TNFα: Tumor Necrosis Factor α

V-CAM1: Vascular Cell Adhesion Molecule 1

VLDL: Very Low Density Lipoprotein

WT: Wild Type

HET→LDLR-/-: LDLR-/- mice that were transplanted with bone marrow from HET mice.

Abstract

Introduction: Increased activation of inflammatory pathways is associated with elevated metabolic stress, which leads to a constellation of metabolic pathologies like fatty liver, insulin resistance and atherosclerosis. Interferon regulatory factor 2 binding protein 2 (IRF2BP2) is a novel transcription co-factor that binds to and inhibits two main pro-inflammatory transcription factors, IRF2 and NFAT1. IRF2BP2 genetic variants are also linked to increased human serum cholesterol level in GWAS studies. Therefore, we **hypothesized** that IRF2BP2 may inhibit macrophage polarization to pro-inflammatory phenotype and considering the remarkable overlap between inflammatory and metabolic sensors, alter their metabolic function. We sought to determine if specific ablation IRF2BP2 in the mouse myeloid lineage (IRF2BP2MKO) leads to development of metabolic symptoms and alters the risk of atherosclerosis.

Results: Our results indicate that IRF2BP2 ablation impairs macrophage polarization to the anti-inflammatory phenotype. IRF2BP2MKO bone marrow derived macrophages (BMDM) show increased oxidized LDL-cholesterol uptake and decreased cholesterol efflux. Also, mice with specific ablation of IRF2BP2 in macrophages are more susceptible to obesity, insulin resistance and hepatic steatosis compared to control mice, when fed high fat diet (HFD). However, LDLR-/- mice transplanted with IRF2BP2MKO bone marrow demonstrate similar atherosclerotic lesions compared to LDLR-/- mice transplanted with control bone marrow, reflecting increased IRF2BP2MKO macrophage apoptosis.

Conclusion: In conclusion, this is the first study to identify the metabolic and inflammatory functions of IRF2BP2 protein in macrophages, with important implications in metabolic syndrome and atherosclerosis.

Chapter 1. Introduction

Atherosclerosis contributes to cardiovascular and cerebrovascular diseases, two of the top five leading causes of deaths in Canada (Statistics Canada, CANSIM table 102-0561). Although novel treatments have reduced the number of deaths related to atherosclerosis, it still remains the most important contributor to cardiovascular mortality. Metabolic syndrome consists of a combination of medical conditions that doubles the risk of cardiovascular diseases (Denton and Spencer, 2010). It affects about 19.1% of the population in Canada and accounts for a significant rate of mortality and morbidity (Riediger and Clara, 2011). Key features of metabolic syndrome are central obesity, hypertension, high fasting blood glucose and atherogenic dyslipidemia. Within components of metabolic syndrome, ATP III[1] identifies elevated low-density lipoprotein (LDL)-cholesterol as one the major risk factors of cardiovascular disease (CVD) (Grundy et al., 2004). On the other hand, elevated circulating LDL is one of the most significant modifiable risk factors for coronary artery disease (CAD) (Wilson et al., 1998).

1.1 Overview of lipid metabolism

Alteration in physiologic lipid metabolism leads to a variety of metabolic disorders, ranging from dermatologic lesions to multi-system pathologies manifested in metabolic syndrome. Cholesterol and triglycerides are the main lipids circulating in plasma within lipoproteins. Major lipoproteins are chylomicrons, very low density lipoprotein (VLDL), intermediate density lipoprotein (IDL), low density lipoprotein (LDL) and high density

[1] The National Cholesterol Education Program's Adult Treatment Panel III report

lipoprotein (HDL). They have a hydrophobic core containing triglycerides and cholesterol esters and a hydrophilic outer layer consisting of apolipoproteins, phospholipids and free cholesterol.

Triglycerides, phospholipids, cholesterol and cholesterol esters absorbed by enterocytes assemble with aoplipoprotein (Apo) B48 to form chylomicrons. Chylomicrons travel within the lymphatic system and then enter the blood stream where they aquire ApoCII from HDL particles. Endothelial cells of the vessel wall synthesize lipoprotein lipase that catalyzes the hydrolysis of triglycerides from chylomicrons into free fatty acids and glycerol which are adsorbed and consumed or stored by peripheral cells (Hegele, 2009),(Charlton-Menys and Durrington, 2008). Chylomicron remnants are taken up and hydrolyzed by hepatocytes.

In the hepatocytes, triglyceride and cholesterol are assembled with ApoB100 to form VLDL. Triglycerides in VLDL are also hydrolyzed by lipoprotein lipase that modifies VLDL to IDL. In turn, IDL is hydrolyzed by hepatic lipase and gives rise to LDL. LDL, which has high cholesterol content, gets endocytosed by liver or other peripheral tissues through interaction with LDL receptor (LDLR) (Charlton-Menys and Durrington, 2008; Hegele, 2009).

ApoA1-containing HDL mediates the reverse transport of cholesterol from the periphery to the liver through its interaction with ABCA1 (ATP-binding cassette A1) and ABCG1 (ATP-binding cassette G1). HDL cholesterol is absorbed into hepatocytes mainly through scavenger receptor B1 (SRB1) (Charlton-Menys and Durrington, 2008; Hegele, 2009).

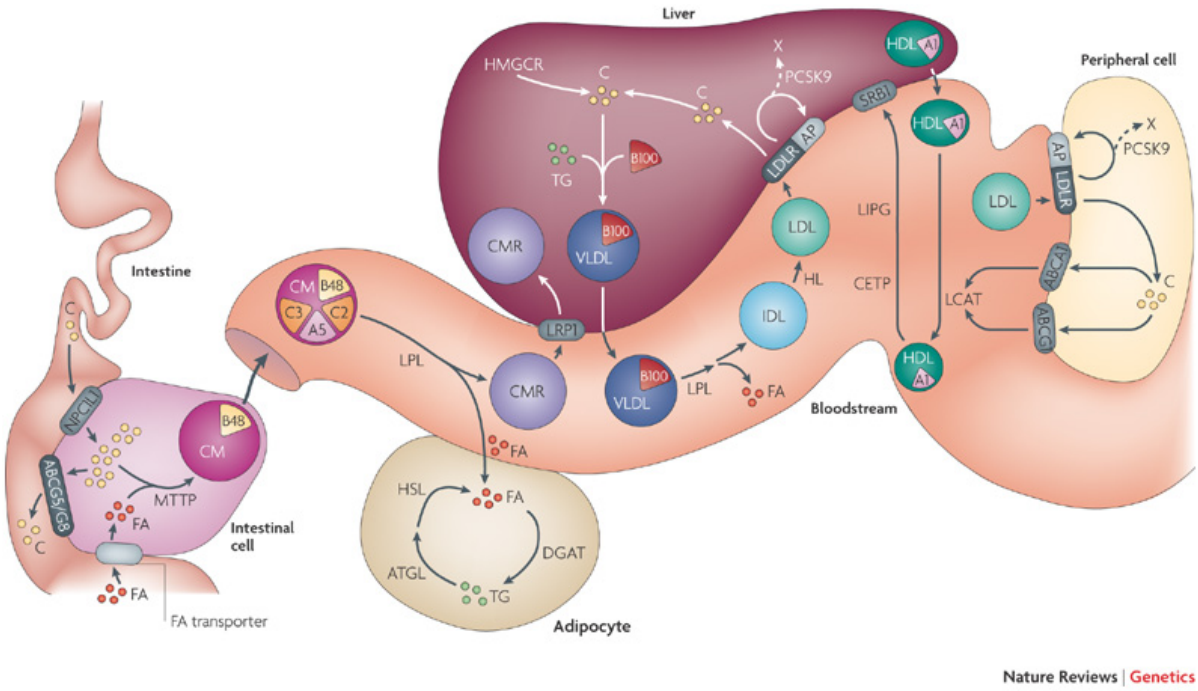

Hegele RA, *Nature Reviews Genetics*, 2009. License number: 3398280547952

Figure 1: Overview of lipid metabolism. CM: chylomicrons. CMR: chylomicron remnants. FA: fatty acids. LPL: lipoprotein lipase. TG: triglycerides.

1.2 Atherosclerotic plaque formation

High levels of circulating LDL cause LDL particles to exit the blood stream and enter the blood vessel subendothelial region where they accumulate. In contact with myeloperoxidase and lipoxygenase, LDL particles undergo oxidative modifications. Modified lipids provoke endothelial cells to release pro-inflammatory factors and adhesion molecules such as E-selectin and V-CAM1 (vascular cell adhesion molecule 1). When adhered to the endothelium, inflammatory cells transmigrate through the endothelium and enter the intima. CCL2 (chemokine (C-C motif) ligand 2, also known as MCP1, monocytes chemotactic protein 1) is an essential monocyte chemoattractant in this process. Other

chemokines, such as CCL5, CCL10 and CX3CL1 (Chemokine (C-X3-C Motif) Ligand 1) attract T-lymphocytes, neutrophils and mast cells into the vessel wall (Libby et al., 2002; Insull, 2009; Hansson and Hermansson, 2011).

Once in the vessel wall, monocytes differentiate to macrophages, which in turn take up oxidized LDL (oxLDL) with their scavenger receptors and develop into foam cells. Over time, accumulation of lipids and recruitment of macrophages continues as well as the inflammatory process. Different inflammatory mediators like interferon-γ (IFNγ) and tumor necrosis factor-α (TNFα) are released in addition to proteases, eicosanoids and other cytokines. Activated leukocytes, endothelial cells and smooth muscle cells release fibrogenic factors and smooth muscle growth factors, which cause proliferation of smooth muscle cells and development of a more advanced and dense lesion.

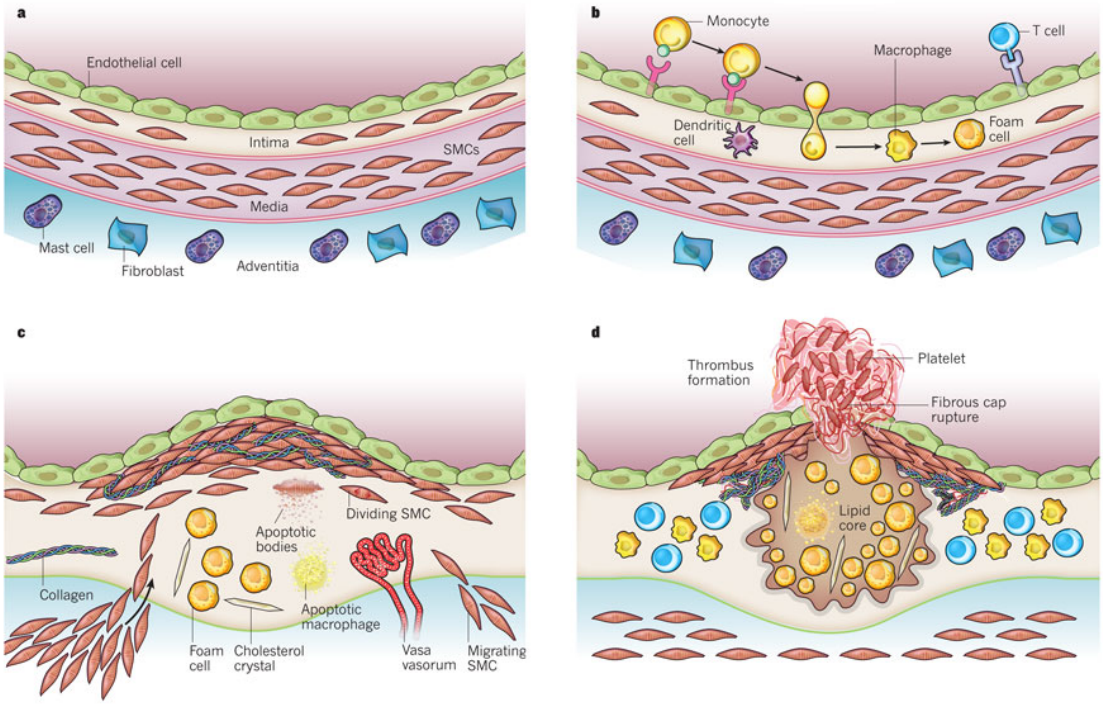

Libby P. *Nature*, 2011. License Number: 3398311038565

Figure 2: Atherosclerotic plaque formation. Images a to d show progression of plaque to more advanced forms.

Continuous enlargement of a more complex lipid pool causes cell necrosis. Cell debris, cholesterol crystals and necrotic cells form a necrotic core in the lesion that is covered and stabilized by a fibrous cap (Insull, 2009; Hansson and Hermansson, 2011).

Activated macrophages in the atheroma release matrix degrading proteolytic enzymes that make the fibrous cap susceptible to rupture by degrading the supporting layer of collagen. IFNγ further inhibits the collagen synthesis and renewal by smooth muscle cells (Libby et al., 2010). Rupture of plaque triggers thrombus formation around the plaque and leads to acute stenosis of the blood vessel. Moreover, tissue factor produced by macrophages induces the thrombosis within the plaque (Libby et al., 2002). Although in real life situations, the cycle of rupture, thrombosis and healing can be repeated several times in the vessel wall, which gives rise to layers of lesion narrowing the lumen (Insull, 2009).

1.3 Inflammation and atherosclerosis

Innate Immunity is defined as the generally non-specific first line of defense against pathogens. Phagocytes like macrophages and dendritic cells play an important role in this process. Adaptive (or acquired) immunity is characterized by elimination of pathogens mediated by antigen specific recognition of pathogens and release of antigen specific antibodies. Lymphocytes are the major players in the adaptive immune response (Akira et al., 2006).

Inflammation is involved in all steps of atherosclerotic plaque formation. Components from both innate and adaptive immunity take part in the process. Different types of immune

cells like macrophages, dendritic cells, neutrophils and mast cells are recruited to the artery wall. Many of the cells express pattern recognition receptors (PRPs) like the Toll-like receptors (TLRs), which bind to oxLDL (TLR2), or minimally modified LDL (TLR4) and activate intracellular inflammatory response. Macrophages are essential in the initiation, maintenance and progression of the inflammatory state in the atherosclerotic lesion. Their role will be discussed more extensively, later in this chapter.

It is now known that oxLDL is not the only trigger of inflammation. Other lipoproteins like VLDL can undergo oxidation and activate endothelial cells. HDL particles are believed to suppress the inflammatory triggers by transporting antioxidant and breaking down the oxidized lipoproteins. Moreover, other risk factors of atherosclerosis like hypertension, diabetes and obesity elicit inflammation. For example, angiotensin II (a potent vasoconstrictor important in the pathophysiology of hypertension), can elicit the production of reactive oxygen species from endothelial cells and the secretion of interleukin-6 (IL-6) and MCP-1 from the smooth muscle cells (Libby et al., 2002).

Adaptive immunity is also present in all stages of atherosclerosis. The importance of lymphocytes was highlighted in a study where apolipoprotein E null (ApoE-/-) mice that were crossed with lymphocytes deficient mice (also known as severe combined immunodeficient mice) had less atherosclerosis (Reardon et al., 2001; Hansson and Hermansson, 2011). T helper 1 (TH1) cells are essential elements present in the plaque. Their main cytokine, IFNγ is atherogenic. Activated CD8+ cells are also reported to increase atherosclerosis in ApoE-/- mice. Although B cells are seldom present in the atherosclerotic lesions, a protective role for these cells in early as well as late stage of atherosclerosis was demonstrated in a study where bone marrow transplanted from B cell deficient mice to LDLR-/- mice (Hansson and Hermansson, 2011).

1.4 Myeloid progeny and macrophages

The first myeloid progenitor derived from stem cells is called Granulocyte-Erythrocyte- Megakaryocyte-Macrophage Colony Forming Unit (GEMM-CFU). Graunolocyte-Monocyte CFU is then derived from these cells and forms the myelomonocytic lineage. Subsequently, monocyte colony stimulating factor (M-CSF) induces the differentiation of monocytic precursors, first to promonocytes and then to mature monocytes. Monocytes leave the bone marrow and enter the blood stream and from there, they reside in different tissues. Their function thereafter will depend on the type of tissue they are residing in and it usually includes a phagocytic role. In each tissue, macrophages have distinct phenotypes and their proliferative status is independent of bone marrow. Examples of tissue macrophages are Kupffer cells in the liver, microglia in the brain, osteoclasts of bone and Langerhans cells of the skin (Valledor et al., 1998).

1.5 Macrophages are key players in metabolic pathologies

Macrophages are essential in metabolic homoeostasis. Resident macrophages in different tissues respond to metabolic stimuli. Metabolites such as fatty acids and cholesterol crystals induce pro- and/or anti-inflammatory mediators (Bhargava and Lee, 2012). Increased activation of inflammatory pathways is associated with elevated metabolic stress, which leads to a constellation of metabolic pathologies like fatty liver, insulin resistance and atherosclerosis (Bhargava and Lee, 2012).

In the systemic circulation, macrophages perform an essential function to take up and remove oxLDL. Macrophages degrade the damaged apolipoprotein and release cholesterol

back into the circulation. Cholesterol is then transported in the form of HDL to the liver where it is excreted in bile salts. However, if cholesterol accumulates in the macrophages due to excess uptake of modified LDL or due to impaired cholesterol efflux, macrophages become the foam cells of atherosclerotic plaque (Ouimet and Marcel, 2012). Macrophage foam cells produce high levels of inflammatory cytokines and chemokines that recruit circulating monocytes that differentiate into more macrophages at the atherosclerotic lesion, leading to further plaque formation and artery occlusion.

1.6 Macrophage polarization: phenotypes and diseases

Depending on the environmental cues, cultured macrophages can become polarized into an inflammatory M1 phenotype or an anti-inflammatory M2 phenotype. Exposure of human monocytes to granulocyte macrophage-colony stimulating factor (GM-CSF) stimulates the formation of inflammatory M1 macrophages, whereas exposure to M-CSF favors M2 non-inflammatory macrophages (Verreck et al., 2004; Verreck et al., 2006). Similarly, exposure to bacterial lipoplolysaccharide (LPS) or IFNγ favors the M1 phenotype, whereas exposure of monocytes to interleukin-4 (IL-4) favors the M2 phenotype. Nuclear factor κB (NFκB), activator protein-1 (AP-1), interferon regulatory factor 3 (IRF3), IRF5, Stimulator of Activated T-cells 1 (STAT1) and STAT2 are among the key transcription factors that skew macrophages to the M1 phenotype (Lawrence and Natoli, 2011). Several transcription factors are implicated in macrophage M2 differentiation, including the Krüppel-like factor 4 (KLF4) (Sharma et al., 2012), nuclear receptor 4A1 (NR4A1 aka Nur77) (Hanna et al., 2012) and peroxisome proliferator-activated receptor delta (PPARdelta) (IJpenberg et al., 1997; Bojic et al., 2012). KLF2 is another transcription factor reported to inhibit NFκB

and AP-1 transcription activity and suppress the expression of pro-inflammatory genes (Das et al., 2006).

The M1 and M2 phenotypes represent two extremes of macrophage differentiation and their contribution to different components of metabolic syndrome has been the subject of extensive investigation. For instance, in obese mice and humans, adipose tissue macrophages (ATMs) are found more in the M1 form, which express pro-inflammatory cytokines like TNFα and iNOS. ATMs of lean subjects on the other hand, show upregulation of M2 markers such as IL-10, Arginase-1 and Ym-1 (Sica and Mantovani, 2012) (Lumeng et al., 2007). Interestingly, Prieur *et al.* showed that M2 ATMs are found in early stages of adipose tissue progression, but more advanced stages of adipose tissue expansion are characterized by a phenotypic switch of ATMs to M1 (Prieur et al., 2011).

Individuals with insulin resistance have higher levels of pro-inflammatory cytokines like TNFα and IL-6. It has been reported that neutralization of TNFα improves insulin sensitivity in obese rodents (Olefsky and Glass, 2010). It has also been shown that the insulin-sensitizing function of adiponectin and leptin are neutralized by pro-inflammatory cytokines from M1 ATMs, causing insulin resistance (Sica and Mantovani, 2012) (Lumeng et al., 2007).

In liver, Kupffer cells secrete inflammatory cytokines in response to high fat diet feeding which causes insulin resistance in liver and promotes liver steatosis. Blocking M2 phenotype has been shown to increase insulin resistance and suppress liver fatty acid oxidation (Kang et al., 2008; Huang et al., 2010). In another study it has been shown that depletion of Kupffer cells inhibits diet-induced insulin resistance and hepatic steatosis. When Kupffer cells were induced to polarize to M1, oxidation of fatty acids was decreased and hepatic fatty acid and triglyceride esterification was increased (Huang et al., 2010).

1.7 Macrophages: Role in atherosclerosis

Recruitment of monocytes into the vessel wall is followed by their differentiation to macrophages in response to cues like M-CSF. TLRs recognize oxLDL and activate the intracellular pathways leading to the production of pro-inflammatory mediators. On the other hand, scavenger receptors take up modified LDL particles and enhance cholesterol accumulation (Yan and Hansson, 2007). In addition to surface receptors, intracellular receptors like nucleotide-binding domain and leucine-rich repeat family, pyrin domain containing 3 (NLRP3) can be activated by cholesterol crystals, and induce the secretion of IL-1 and IL-18 (Hansson and Hermansson, 2011). This vicious cycle of inflammation then continues by recruiting more immune cells to the lesion producing more chemokines. Although various characters of macrophages have been investigated extensively, I will focus on three aspects of their function, macrophage cholesterol metabolism, macrophage polarization and macrophage apoptosis.

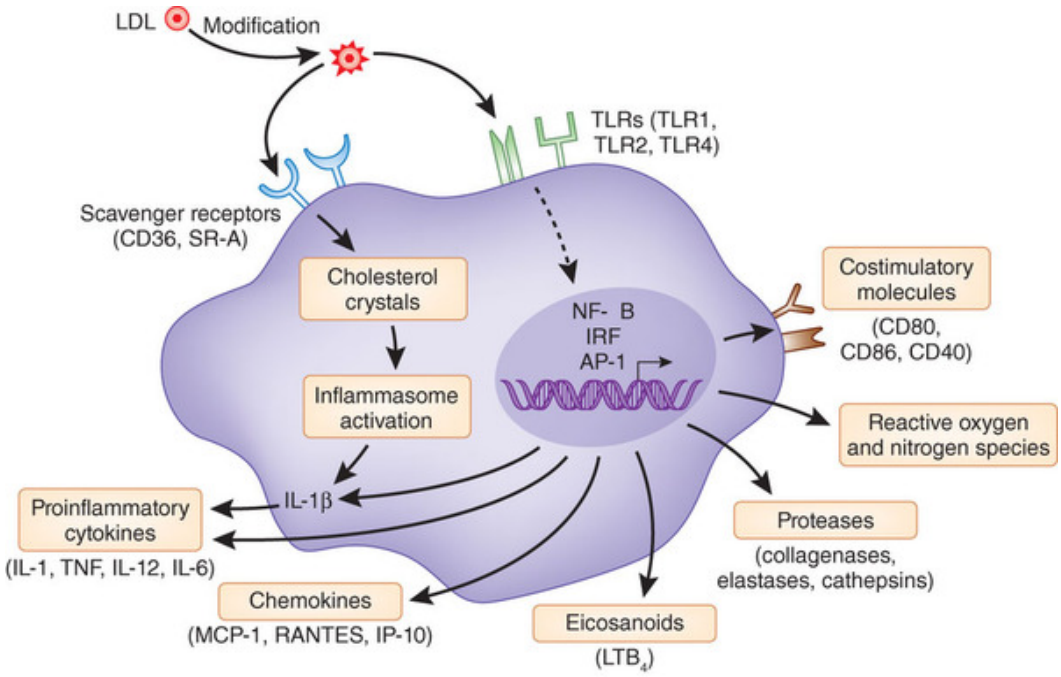

Katie Vicari, from Hansson GK, *Nature Immunology*, 2011. License number: 3398291124592

Figure 3: Activation of macrophages and pathways leading to a pro-inflammatory phenotype.

1.7.1 Macrophage cholesterol homeostasis

Cholesterol uptake - Macrophages are key players in the whole body cholesterol metabolism. Moreover, their cholesterol uptake and transport is essential in the progression of atherosclerotic lesions.

Macrophages internalize lipoproteins via several types of receptors including scavenger receptors, LDL Receptor (LDLR), VLDL receptor, and LDLR-related protein (LRP) (Pennings et al., 2006). Uptake through LDLR is performed by the interaction of ApoB100 with LDLR and internalization of the lipoprotein by the cell. It was previously believed that since the sterol content of the cell regulates the expression of LDLR, uptake through this pathway does not lead to uncontrolled lipid accumulation (Vainio and Ikonen,

2003) and yet has a limited role in atherosclerosis development. But evidence suggests that macrophage LDLR enhances atherosclerosis (Pennings et al., 2006).

Scavenger receptors are members of the PRP family of receptors and are categorized into several classes. In addition to the recognition and uptake of a broad range of ligands including pathogens, they facilitate internalization of LDL that is modified by acetylation, oxidation or enzymatic digestion. This type of uptake is not controlled by the intracellular cholesterol level (Vainio and Ikonen, 2003). Not only is LDL uptake through these receptors the major route for foam cell formation, it also triggers the activation of a macrophage pro-inflammatory phenotype (Moore and Freeman, 2006).

The class A scavenger receptors, SR-A1 and SR-A2 are believed to uptake about 80% of the AcLDL (a modified LDL that does not exist *in vivo*) with lower affinity for oxLDL. The proatherogenic role of this class of scavenger receptors is established by studies that reported a 20% to 80% reduction of atherosclerotic lesion size after ablating SRA-1 and SRA-2 in APOE-/- or LDLR-/- mice (Moore and Freeman, 2006; Pennings et al., 2006). Furthermore, these receptors play an important role in advanced stages of atherosclerosis where their pathway leads to excessive accumulation of free cholesterol, causes ER stress, and ultimately apoptosis (Moore and Freeman, 2006).

Among Class B scavenger receptors, CD36 and SR-B1 are better known for their role in foam cell formation. CD36 has a high affinity for moderately oxidized LDL and accounts for about 60% of cholesterol ester accumulation in the macrophages after oxLDL treatment. Ablation of this receptor causes marked reduction in the extent of atherosclerotic lesion (Moore and Freeman, 2006).

SRB-1 is mainly an HDL receptor that facilitates selective uptake of cholesterol ester from HDL particles (Vainio and Ikonen, 2003). In addition to its role in cholesterol uptake, it

is also involved in cholesterol efflux from macrophages. The role of SRB-1 in atherosclerosis therefore seems to be complex. It enhances the formation of fatty streaks. However, it reduces the advanced atherosclerotic lesions in ApoE-/- or LDLR-/- mice (Pennings et al., 2006).

Lectin-type oxidized LDL receptor 1 (LOX1), also known as Oxidized LDL Receptor 1 (OLR1), belongs to class E scavenger receptors (Moore and Freeman, 2006). It is activated not only by oxLDL, but also with Angiotensin II, and therefore LOX1 is viewed as a key link between dyslipidemia and hypertension (Mitra et al., 2011). Although whole body ablation of LOX1 has been reported to reduce atherogenesis in LDLR-/- mice (Mehta et al., 2007), the specific atherogenic effect of LOX1 deficient macrophages has not been investigated.

Cholesterol Efflux – Cholesterol efflux is the first step in the process of reverse cholesterol transport. It is the main mechanism through which macrophages expel their excess cholesterol. Since cholesterol is stored mainly in the form of esterified cholesterol, and only free cholesterol is suitable for efflux, cholesterol needs to be hydrolyzed before efflux (Vainio and Ikonen, 2003).

In macrophages, cholesterol efflux occurs through three routes. The first and most important route of cholesterol efflux occurs when cholesterol is transferred from the cell membrane to acceptor lipoprotein particles mediated by membrane proteins. Second, macrophages can efflux cholesterol together with the ApoE they produce. The third pathway, which is the least significant route of efflux, involves the conversion of cholesterol to 27-hydroxycholesterol by P450-dependent cholesterol oxidases (Cavelier et al., 2006).

ATP-binding cassette A1 (ABCA1) protein is the key transporter in cholesterol efflux. It facilitates lipid transfer to ApoA1 and takes part in the formation of HDL particle.

Therefore, its function is important in the maintenance of HDL level in the blood stream. ABCG1, which is the second transporter in the same family, further assists ABCA1 in the maturation of the HDL particles. Expression of these two transporters is regulated by LXR (Liver X Receptor). Simultaneous ablation of these two transporters in macrophages leads to enhanced atherogenesis (Pennings et al., 2006; Ikonen, 2008).

1.7.2 Macrophage polarization

Both M1 and M2 macrophages are present in the atherosclerotic lesion. TH1 cells, which are highly present at the lesion site, produce IFNγ and induce the M1 macrophage phenotype. In addition, oxLDL and necrotic debris induce inflammatory activation. On the other hand, activation of the downstream LXR pathway by accumulation of oxysterol inhibits NFκB signaling and induces expression of arginase 1, skewing macrophages to the M2 phenotype. Th2 cells as well as intra-lesional hemorrhage induce M2 polarization by producing antiatherogenic IL-10. Therefore the balance between the entire spectrum of macrophage activation affects the outcome of atherosclerosis (Mantovani et al., 2009).

Of note, KLF4-deficient macrophages which exhibit enhanced inflammatory activation (M1) and foam cell formation in response to oxLDL cause more atherosclerotic lesion formation in ApoE-/- mice (Sharma et al., 2012). Similarly, NR4A1-deficient macrophages display an inflammatory phenotype (M1) that worsens atherosclerosis in susceptible mice (Hanna et al., 2012). Thus, reduced expression of transcription factors that suppress the inflammatory phenotype are predicted to worsen foam cell formation and atherosclerosis.

1.7.3 Macrophage apoptosis

The necrotic core is a critical feature within a plaque that can lead to breakdown of the fibrous cap, inflammation and thrombosis. Necrosis occurs when macrophages in the advanced lesion become apoptotic and there is a simultaneous defect in the phagocytic clearance capacity within the plaque (Moore and Tabas, 2011). Efferocytosis is defined as the phagocytic removal of apoptotic/necrotic bodies, and it is defective in the later stages of atherosclerosis, which contributes in the core of the plaque becoming necrotic.

Early apoptosis: Although macrophage apoptosis happens throughout different stages of atherosclerosis, its appearance in early vs. late lesions has distinct implications (Tabas, 2005). The trigger for early apoptosis is not well known. However, studies that investigated the effect of altered early macrophage apoptosis demonstrated that increased apoptosis leads to smaller and less progressive lesions (Tabas, 2010). For example, Arai *et al.* showed that increasing macrophage apoptosis in double KO mice, AIM-/-LDLR-/-, decreases the early lesion development (5 weeks of western diet) as well as late lesion areas (12 weeks of western diet) (Arai et al., 2005). Liu et al. used ablation of Bax as a mean to reduce apoptosis in macrophages. Transplantation of Bax-/- bone marrow to LDLR-/- mice resulted in significant increase in the mean lesion area compared to LDLR-/- mice transplanted with WT bone marrow after 10 weeks of western diet feeding (Liu et al., 2005). Similarly, transplantation of Prostaglandin E2 (PGE2) receptor E4 (EP4)-deficient bone marrow to LDLR-/- mice resulted in decreased macrophage survival and suppressed early atherosclerosis after 8 weeks western diet (Babaev et al., 2008).

Efferocytosis seems to be efficient at early stages when macrophage apoptosis occurs. Beneficial effects of successful efferocytosis include prevention of toxic material

leak from dead cell particles and induction of anti-inflammatory signals including IL-10 and TGFβ. Thus, the efferocytes survival is enhanced which promotes efflux of proapoptotic modified LDL and an overall stable lesion (Moore and Tabas, 2011).

Late apoptosis: A combination of elements contributes to macrophage death in the later stages of atherosclerosis. Oxidative stress, activation of death receptors, persistent activation of endoplasmic reticulum (ER) stress pathways and deprivation from growth factors, presence of toxic cytokines are among the important triggers (Tabas, 2010; Moore and Tabas, 2011).

Studies of human coronary artery disease established a correlation between expression of ER stress proteins with plaque vulnerability and apoptosis. One of the pathways activated by ER stress induces expression of CHOP (CEBP-Homologous Protein), which in turn triggers apoptosis through several mechanisms. ER stressors are either strong enough to cause apoptosis, or they do so in combination with another signal. Among the most well studied signals are activation of PRPs and excessive cholesterol accumulation within the cell (Tabas, 2010).

Defective efferocytosis is what makes late apoptosis more threatening than early macrophage apoptosis. It is unclear why efferocytosis is not sufficient in more advanced lesions. Examples of the suggested underlying causes are: reduction in the total pool of efferocytes, poor exhibition of efferocyte ligands by apoptotic cells, defect in the function of bridging molecules and efferocyte receptors, or changes introduced by the process of aging (Tabas, 2010). Thus the decrease in the phagocytosis of dead cells ultimately leads to augmentation of pro-inflammatory signals and generation of a necrotic core (Tabas, 2005).

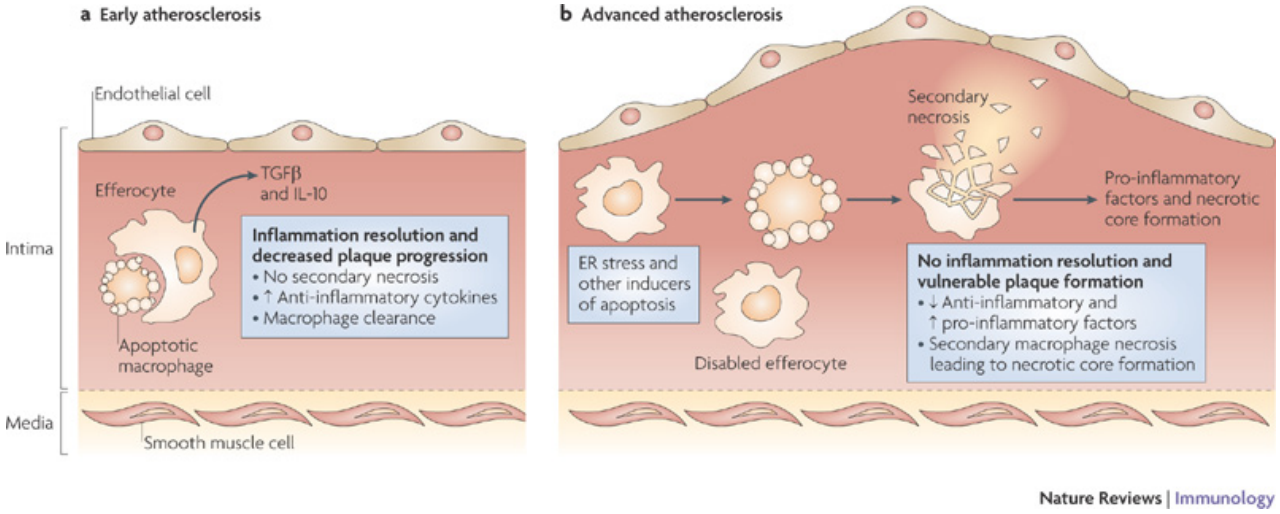

Tabas I, *Nature Reviews Immunology*, 2010. License number: 3398300162540

Figure 4: Disabled efferocytosis contributes to necrosis and plaque vulnerability.

1.8 IRF2BP2, and the indirect link to innate immunity

Interferon Regulatory Factor 2 Binding Protein 2 (IRF2BP2) is a 587 amino acid protein that belongs to a 3-gene family of transcription cofactors (IRF2BP1, IRF2BP2 and IRF2BPL), containing a single N-terminal C4 zinc finger and a C-terminal C3HC4 RING domain. These domains are >90% identical among members of the family (IRF2BP1, IRF2BP2 and EAP1) (Yeung et al., 2011). The zinc-finger motif is involved in homo and hetero-dimerization of IRF2BP2 family members. The RING-finger motif interacts with Interferon Regulatory Facor-2 (IRF-2) as well as Nuclear Receptor Interacting Factor 3 (NRIF3) (Tinnikov et al., 2009; Teng et al., 2011).

IRF2BP2 is a member of a gene family with related structure yet different function. IRF2BP1 is reported to be an IRF-2 co-repressor. It also functions as a ubiquitin ligase (Kimura, 2008). EAP1 is suggested to play a role in controlling female reproductive system by its function in the neuroendocrine system (Heger et al., 2007).

IRF2BP2 was initially discovered as a co-repressor of IRF2 (Childs and Goodbourn, 2003). IRF family is a family of transcription factors that contains IRF-1, IRF-2 and seven other members. IRF-1 is strongly induced by IFN-γ and binds to IFN-stimulated responsive elements (ISREs) within promoters, which leads to activation of transcription. These ISREs, located within promoters of many IFN-mediated genes, are usually defined by palindromic TTTC sequences separated by two or three nucleotides. On the contrary, IRF-2 is constitutively expressed and reported to act mostly as a repressor, competing with IRF-1 for the same cis-element (Blanco et al., 2000). However, evidence showed that IRF-2 also functions as a transactivator. IRF-$2^{-/-}$ mice analysis showed that like IRF-1, IRF-2 is required for normal generation of Th1 responses. Thus, it has been suggested that IRF-1 and IRF-2 may act as functional agonists rather than antagonists on some IFN-γ-responsive genes (Elser et al., 2002). Dysregulated nitric oxide (NO) release and IL12 gene induction have been reported for IRF-2–deficient macrophages (Blanco et al., 2000). IRF2 is also shown to transcriptionally repress IL4, a Th2 cytokine (Elser et al., 2002), but it negatively regulates Cox2 promoter (Blanco et al., 2000). IRF2BP2 has been shown to interact with the c-terminal domain of IRF2 and act as IRF2-dependent transcriptional corepressor (Childs and Goodbourn, 2003).

NFAT1 is a member of the NFAT family of transcription factors. It is a key player in the regulation of cytokine gene transcription and the immune response. NFAT family's central feature of regulation inferred from their marked sensitivity to the immunosuppressive drugs cyclosporin A (CsA) and FK506 (Tacrolimus). NFAT1 is also essentially involved in transcriptional regulation of proinflammatory genes such as IL2 and TNFα. NFAT was recently reported to be activated upon LPS stimulation of murine microglia cells and NFAT inhibition with tat-VIVIT peptide decreased LPS induced TNF alpha and MCP1 secretion

(Nagamoto-Combs and Combs, 2010). IRF2BP2 binds to NFAT1 (IRF2BP2 RING domain with NFAT1 C terminal domain) and repress the expression of TNF alpha, IL2 and IL4 in Jurkat T cells (Carneiro et al., 2011). Although RING domains are generally considered to be involved in the ubiquitination and protein degradation pathway, IRFBP2 interaction with NFAT1 does not lead to NFAT1 degradation (Carneiro et al., 2011).

Based on its binding to IRF2 and NFAT1 proteins which promote pro-inflammatory responses, we hypothesized that IRF2BP2 may inhibit macrophage polarization to M1.

1.9 IRF2BP2 identified in several GWAS

Two GWAS identified variants in the vicinity of IRF2BP2 that associate with elevated plasma LDL-C in individuals of European-ancestry (rs514230, risk allele frequency=48%) (*P* value: 5.37×10^{-14} for total cholesterol and 9.4×10-12 for LDL-C) (Teslovich et al., 2010) and of black African ancestry (rs744487, raf=72%) (*P* value: 5×10^{-6}) (Lettre et al., 2011). Another GWAS identified another variant in the vicinity of IRF2BP2 (rs482329, raf=64%) that is associated with life threatening arrhythmias (Murray et al., 2012) (*P* value: 5.5×10^{-6}). Although these studies did not determine whether these variants were associated with altered IRF2BP2 expression, these studies suggest that IRF2BP2 may participate in the progression of ischemic heart disease, a process that would also depend on worsening coronary atherosclerosis through macrophage foam cell formation and dysregulated hepatic LDL-C homeostasis.

Inflammation plays an indisputable role in the development of metabolic syndrome and atherosclerosis. However, we do not fully comprehend the transcriptional regulatory

network that controls inflammation. The **first aim** of this study was to evaluate the effect of myeloid-specific ablation of IRF2BP2 on macrophage polarization. This is the first study that establishes the role of IRF2BP2 in macrophage inflammatory response. We found that IRF2BP2MKO BMDMs are defective in polarization to anti-inflammatory phenotype (M2). Then, we pursued our **second objective** to determine if IRF2BP2MKO mice show symptoms of metabolic syndrome, altered cholesterol metabolism or atherosclerosis. Here we establish that IRF2BP2MKO mice develop obesity, steatohepatitis and cholesterol metabolism deficits when fed high fat diet (HFD). Despite the systemic inflammatory phenotype induced by ablation of IRF2BP2 in macrophages, LDLR -/- mice transplanted with IRF2BP2MKO bone marrow (MKO→LDLR-/-) had similar atherosclerotic lesions to control mice possibly due to increased apoptosis.

Chapter 2. Materials and Methods

2.1 Animal model and animal care

We generated a floxed allele of IRF2BP2 and mated these mice to LysMcre mice that express Cre-recombinase in the myeloid lineage (Clausen et al., 1999). Figure 5 is a schematic diagram showing the process of generating IRF2BP2MKO mice. LysMcre/IRF2BP2$_{flx/flx}$ mice are hereafter referred to as IRF2BP2MKO. Heterozygote mice (HET) used in most experiments were LysMcre IRFBP2$_{flx/wt}$. WT mice used in microarray experiments do not contain LysMcre allele. All procedures carried out in mice were approved by the animal care and use committee of the University of Ottawa. All animals were bred and maintained in the University of Ottawa animal facility under a 12-hour light (0600-1800) and 12-hour dark (1800-0600) cycle. Food (regular chow) and water were provided *ad libitum* unless specified.

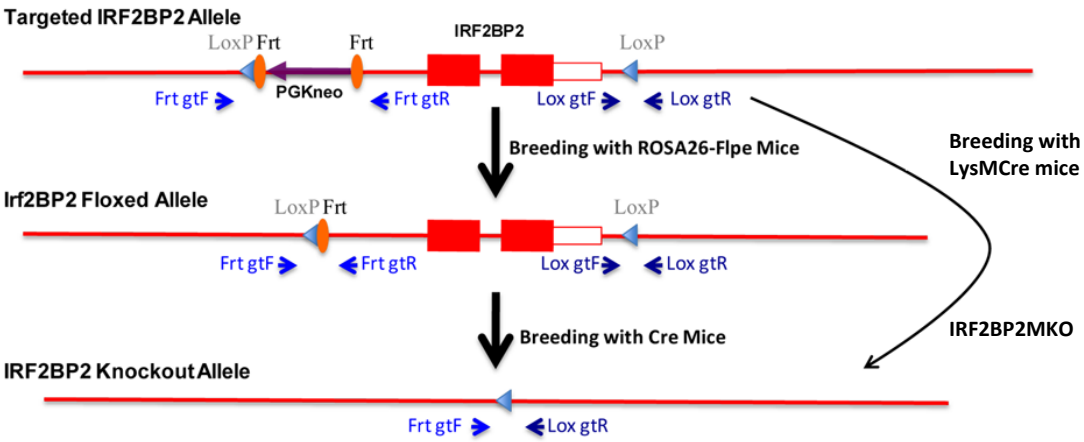

Figure 5: A schematic diagram showing the process of generating of IRF2BP2MKO mice.

2.2 Cell culture

For harvesting BMDM, briefly, two femurs and two tibias from each mouse were flushed with medium, and cells were centrifuged at 1400 g for 5 min, re-suspended in BMDM medium (20% FBS, 15% L929 conditioned medium, pen/strep, glutamine), and seeded in non-tissue culture treated plates (BD Falcon) for 6 days. Medium was changed at DIV3. Cells were then stimulated with LPS 100ng/ml (Sigma) or IL4 5ng/ml (Sigma) and harvested for mRNA and protein analysis. For cholesterol metabolism studies, BMDMs were cultured from IRF2BP2MKO or wild type mice as controls. L929 conditioned medium was collected from the L929 cells cultured for 7 days, centrifuged at 2000g for 5 min and filtered through 0.45μm low protein binding filter.

F11 cells are hybrid cells of rat embryonic dorsal root ganglion cells and mouse neuroblastoma cells. RAW 264.7 cells are mouse leukemic monocyte macrophage cell line. Both F11 and RAW 264.7 were cultured in DMEM containing penicillin, streptomycin and glutamine with 10% FBS.

2.3 Cholesterol uptake, cholesterol efflux and cholesterol content

BMDMs were treated with oxLDL (30μg/ml, Biomedical Technologies, Inc) for 48 hours, then washed with PBS and fixed with 4% paraformaldehyde for 0.5 hour. The cells were then washed one time with PBS, one time with 60% isopropanol and incubated with 0.3% Oil Red O in 60% isopropanol for one hour, washed two times with PBS and one time with 60% isopropanol. BMDMs grown on coverslips were stained with 4',6-diamidino-2-phenylindole (DAPI) and mounted after staining for imaging purposes.

For quantification of cholesterol uptake, AcLDL 50 μg/ml was pre-incubated with ^{3}H-cholesterol 1 μCi/ml for 16 hours at 37 °C before the experiment. BMDMs were treated with ^{3}H-cholesterol containing AcLDL for 30 minutes. The cells were then washed two times with PBS, lysed with 0.5N NaOH for two hours at room temperature. Aliquots of cell lysate from each condition (200μl) were mixed with 1 ml ScintiSafe Gel (Fisher Scientific) and the radioactivity was measured for 1 minute per sample. The values were normalized to the protein amount of BMDMs cultured simultaneously in separate dishes.

For efflux quantification, BMDMs were treated with ^{3}H-Cholesterol (PerkinElmer) 1 μCi/ml for 48 hours and then washed with PBS and incubated with HDL 50μg/ml (Biomedical Technologies, Inc) or ApoA1 30 μg/ml (Biomedical Technologies, Inc). After 4 hours, aliquots of medium from each condition (150μl) were mixed with 1 ml ScintiSafe Gel (Fisher Scientific). Radioactivity was measured for 1 minute per tube and the values were normalized to the radioactivity of the cells lysates (lysed with 0.5N NaOH overnight).

BMDMs were treated with AcLDL 50μg/ml for 24 hours and their cholesterol content (total and free cholesterol) was measured using "Cholesterol/cholesteryl ester quantification colorimetric kit" (Biovision, Catalog # K603-100). Cholesteryl ester was calculated by subtracting free cholesterol from total cholesterol.

2.4 Lipid Profile and ELISA

Wild type and IRF2BP2MKO mice were grouped to receive chow or high fat diet (daily calorie composition of 60% fat, 21% carbohydrate, 19% protein)(Harlan) for 20 weeks. Body weights were measured at the same weekly time. Mice were fasted in new cages overnight for about 16 hours before collecting blood from the saphenous vein. Blood

samples were allowed to clot for 2 hours at room temperature and centrifuged at 10,000g for 10 minutes to separate serum. Collected serum was used for FPLC analysis, total cholesterol assay (VWR, Free Cholesterol E Kit), ApoE ELISA assay, and IL1β ELISA assay (R&D Biosystems) according to the manufacturers' guidelines.

FPLC analysis was conducted using 75µl pooled plasma (n=3 per group) separated on a Superose column (Amersham) with a flow rate of 0.4 ml/min. Mice were fasted for 16 hours before blood collection. Total cholesterol content was measured from collected fractions using the Wako Cholesterol E kit (# 439-17501). From each fraction of about 500 µl, 16 µl was loaded for western blotting and 50 µl was used for measuring the cholesterol content.

2.5 Glucose tolerance test (GTT)

Mice were fasted in new cages overnight for about16 hours with access to water. All tests were started at 10:00 AM. Fasting blood glucose was measured prior to a bolus intra-peritoneal injection of 20% D-glucose 1 g/kg body weight. Blood was sampled from the saphenous vein at 15, 30, 60, and 120 minutes after injection and glucose was measured using a standard glucometer.

2.6 Quantitative real-time PCR

Total RNA from BMDMs was extracted using TRIzol reagent (Invitrogen) or using Qiagen RNeasy Mini Kit (74104) followed by ethanol purification. Then RNA was reverse-transcribed to cDNA with random decamers and M-MLV reverse-transcriptase (Ambion). An aliquot of cDNA was used for qPCR with specific primers or housekeeping gene primers

(GAPDH or cyclophilin) together with Taq DNA polymerase/SYBR Green PCR mix (ThermoScientific) with the Rotor-Gene 3000 System (Corbett Life Science). All mRNA levels were normalized to GAPDH or cyclophilin. Gene specific qPCR primers used are listed in Table 1.

2.7 Microarray study

RNA isolated from individual BMDM cultures from 3 littermate control and 3 IRF2BP2MKO mice (2 months old) for each sex were analyzed for purity and integrity on an Agilent Bioanalyzer and expression profiled on Affymetrix® Mouse Gene ST 1.0 arrays at the StemCore Laboratories in Ottawa Hospital Research Institute.

2.8 Western blotting

Protein extraction and western blot analysis were performed as described previously (Chen et al., 2007). A rabbit antibody against the IRF2BP2 epitope KLEEPPELNRQSPNPRR was custom ordered from OpenBiosystems, affinity purified, and used in immunoblot analysis, as described previously (Teng et al., 2010). Antibodies to CD36, IFNα, KLF2 (Milipore), PPARγ (SantaCruz), ABCA1 (Novus Biologicals), and actin (Sigma) were used. Immunoblots were quantified using the Image J software (NIH).

2.9 Immunofluorescence and TUNEL staining

Cryosections were air dried at room temperature for half an hour, washed three times with PBS and then incubated in 1% Triton X-100 containing PBS for 10-15 minutes. Sections were blocked in 5% donkey serum containing 1% Triton X-100 for 1 hour at room

temperature. Primary antibodies were diluted in 1% donkey serum in PBS containing 1% Triton X-100 and incubated either at room temperature for 3 hours or at 4°C overnight. Slides were washed 5 times each 5 minutes with PBS and then treated with DAPI (4',6-diamidino-2-phenylindole) to stain the nuclei and secondary antibody diluted in 1% donkey serum in PBS containing 1% Triton X-100 for 1 hour at room temperature. The slides were then washed 5 times each 5 minutes and mounted with an aqueous mounting medium (ThermoScientific, 6769006). A serial section was stained with the same procedure without primary antibody to control for any background fluorescent staining. TUNEL staining was performed using Promega TUNEL staining kit (G3250).

Table 1: List of primers used and their annealing temperatures.

Gene	Forward	Reverse	Annealing
ABCA1	CGTTTCCGGGAAGTGTCCTA	GCTAGAGATGACAAGGAGGATGGA	57
ABCA9	ACTCGAAAGAAGAAACGGGAC	GGAAGTAGATGTGAAAGTTCTGAG	54
ABCG1	GAAGTGGCATCAGGGGAGTA	AAAGAAACGGGTTCACATCG	54
Arginase1	GGGAAAGCCAATGAAGAGCTG	AGGAGAAAGGACACAGGTTGC	55
CCL2	CACTCACCTGCTGCTACTCATTC	GCTTCTTTGGGACACCTGCTG	57
CD206	CCCAAGGGCTCTTCTAAAGCA	CGCCGGCACCTATCACA	60
CD36	TCGGATCTGAAATCGACCTT	CACAGGCTTTCCTTCTTTGC	57
CX3CR1	CAGCATCGACCGGTACCTT	GCTGCACTGTCCGGTTGTT	55
KLF2	ACCAAGAGCTCGCACCTAAA	GTGGCACTGAAAGGGTCTGT	58
iNOS	AGCCCTCACCTACTTCCTG	CAATCTCTGCCTATCCGTCTC	59
IL1-β	GCTTCAGGCAGGCAGTATC	AGGATGGGCTCTTCTTCAAAG	56
IL-6	ACCGCTATGAAGTTCCTCTC	CTCTGTGAAGTCTCCTCTCC	54
IRF2BP2	AGTTCTGTTTCCCTTGCTCC	TCTTCACTTTCACATCTCCGG	54
Mgl-1	TGAGAAAGGCTTTAAGAACTGGG	GACCACCTGTAGTGATGTGGG	60
LOX1	CAAGATGAAGCCTGCGAATGA	ACCTGGCGTAATTGTGTCCAC	54
SRA1	CTGGACAAACTGGTCCACCT	TCCCCTTCTCTCCCTTTTGT	57
SRB1	TGCTCAAGAATGTCCGCATA	ACGGTGTCGTTGTCATTGAA	57
Sort1	ACCTGTTAGCTCTCAGCACCGAAA	CAGCTTTGCAGGAGCCATTCACAT	58
Retnlb	TCCAGCTAACTATCCCTCCACTGT	GGCCCATCTGTTCATAGTCTTGA	57
TNFα	GGTTCTGTCCCTTTCACTCAC	TGCCTCTTCTGCCAGTTCC	56
GAPDH	TCTCCTGCGACTTCAACAGC	TGGTCCAGGGTTTCTTACTTC	54-60
Cyclophilin	TGGAGAGCACCAAGACAGACA	TGCCGGAGTCGACAATGAT	54-60
ApoE	GATCAGCTCGAGTGGCAAAG	TAGTGTCCTCCATCAGTGCC	54
YM1	GGGCATACCTTTATCCTGAG	CCACTGAAGTCATCCATGTC	60
PPARg	CAAGAATACCAAAGTGCGATCAA	GAGCAGGGTCTTTTCAGAATAATAAG	59
SREBP1α	TAGTCCGAAGCCGGGTGGGCGCC GGCGCCAT	GATGTCGTTCAAAACCGCTGTGTGT CCAGTTC	59

2.10 Luciferase assay

Briefly, F11 cells in each well of a 12-well plate were transfected with luciferase-expressing vector (400ng), specified expression constructs or corresponding empty vectors (e.g., cDNA3) (100ng) and pCMVβgal (50ng) to normalize the transfection efficiency. PGIPz lentiviral plasmids of mouse IRF2BP2 shRNA (V3LMM_432752: TTCACTTTCACATCTCCGGCGA) and nonsilencing control shRNA (RHS4346) constructs were purchased from OpenBiosystems (Thermo Scientific, Huntsville, AL, USA). Transfection was carried out using Lipofectamine 2000 reagent (Invitrogen), with the 1:2 ratio of total plasmid to Lipofectamine. Cells were collected 24 hours after transfection and lysed with four repeated cycles of snap freezing and thawing. Luciferase and β-galactosidase assays were performed in triplicate.

2.11 Hematoxylin and Eosin (H&E) staining

Tissues were cryo-sectioned at a thickness of 10 µm and slides were air dried for half an hour at room temperature and fixed in methanol at -20 for 10 minutes. Sections were soaked in Hematoxylin solution for 3 minutes followed by running tap water (35°C – 37°C) for 2 minutes, then underwent 10-14 dips in HCl alcohol (70% EtOH + 8 drops HCl) followed by running tap water for 15 minutes. Sections were then soaked in 25% EtOH for 1 min and then underwent 4-6 dips in Eosin solution and then the slides were sequentially dehydrated from 70% EtOH (10 dips) to 90% EtOH for 30 sec followed by 100% EtOH for 2 changes (1 min each) and 100% EtOH: Xylene (1:1 mix) for 1 min. Finally, slides were transferred to Xylene for 1 min and another change of Xylene for 5 min or more before mounting. The slides were then mounted with Permount (Fisher Scientific).

2.12 ApoE and IL1-β ELISA

IL1-β ELISA was performed using R&D Systems mouse IL1-β kit (MLB00C). ApoE ELISA was performed according to the following protocol. Plates (96-well) were coated overnight (100 µl/well) at 4°C with goat anti-ApoE polyclonal antibody (Calbiochem 178479) at a dilution of 1:10000 in sodium bicarbonate buffer (0.05 mmol/L, pH 9.6). After washing twice (200 µl/well) with PBS containing 0.05% IGEPAL CA-630 (Sigma), the wells were blocked (200 µl/well) with 1% bovine serum albumin (BSA) (Sigma, A7030) in PBS for 1 hour at room temperature. Wells were washed twice with PBS containing 0.05% IGEPAL CA-630. Serum samples and standards were diluted 1:200 in PBS containing 0.05% IGEPAL CA-630 and 0.1% BSA. 100 µl/well of samples and standards were added to wells in duplicate for each sample. After 2 hours of incubation at room temperature, wells were washed four times with PBS containing 0.05% IGEPAL CA-630. For detection, wells were incubated for 1 hour at room temperature with rabbit-anti-mouse ApoE (Meridian Life Science Inc. K23100R) diluted 1:1000 in blocking buffer (100 µl/well), washed four times with PBS containing 0.05% IGEPAL CA-630 and incubated for 30 minutes at room temperature with alkaline phosphatase conjugated anti-rabbit IgG antibody (Sigma A9919) diluted at 1:5000 in blocking buffer (100 µl/well), wells were washed four times with PBS containing 0.05% IGEPAL CA-630. Alkaline phosphatase substrate pNitrophenyl phosphate (Sigma, N7653) was added (200 µl/well) and plates were incubated at room temperature for 30 minutes in the dark. Absorbance was measured at 405 nm on a kinetic microplate reader (Molecular Devices). A standard curve was constructed for each plate, using serial dilutions of C57/Bl6J serum and with ApoE knockout mouse serum as a negative control.

2.13 Bone marrow transplantation and quantification of atherosclerotic area

LDLR-/- (from Jackson labs) and donor male mice were given antibiotic (enrofloxacin) in drinking water to the cages 5-7 days prior the transplantation. The day of transplantation, mice were irradiated (gamma type) twice approximately 3 hours apart (4.5 Gy each time, approximately 2 minutes and 45 seconds total) and then placed in sterile caging with sterile acidified water. At the same time donor mice were sacrificed and bone marrow was extracted from their femurs and tibias. In a sterile laminar flow cabinet, 5-7 million viable bone marrow cells are injected into the retro-orbital sinus of the acceptor mice in 0.1 ml of DMEM. Mice were given sterile watersoaked rodent cubes daily to encourage them to eat and stay hydrated (since they lose approximately 20% of their BW in the first 2 weeks). Health wellness/weight checks on the mice was performed 3 times a week for the first 2 weeks and then 2 times per week until the mice return to standard, non-sterile housing at 6 weeks' time.

After 6 weeks recovery, mice were fed with western diet (Harlan, TD88137) for 12 weeks, then anesthetized, blood was drawn, and mice were perfused with 10 ml of PBS and 20 ml of 4% paraformaldehyde in PBS. The aorta was dissected out carefully and placed in 4% paraformaldehyde in PBS overnight. After fixation, aortas were immersed in 20% sucrose in PBS for at least 24 hours. Aortas were then embedded in OCT compound/20% sucrose (1 to 1 volume), and cryo-sectioned. Sections were collected starting from the first appearance of the three cusps of the aortic valve. For each mouse, four sections (10 μm thickness) 100 μm apart were stained with oil-red-O and were used for lesion quantification. Four adjacent serial sections were stained with H&E for histological examination. Additional

sections were stained with macrophage-specific antibodies or with TUNEL for apoptosis quantification.

2.14 Food intake

Mice were transferred to individual metabolic cages and habituated for 24 hours. Food intake study was performed on powdered regular chow and measured daily at 17:00 for 5 days.

2.15 Indirect calorimetry

Mice were individually housed in a four-chamber Oxymax open-circuit indirect calorimeter (Columbus Instruments, Columbus, OH) and had access to food and water *ad libitum*. The chambers were maintained at room temperature (22–23°C) with airflow rate of 0.5 L/min and with a normal light-dark cycle (light 0600–1800, dark 1800–0600). Concentrations of O_2 and CO_2 were measured for 60 seconds every 4 minutes in each chamber with a sample line purge time of 2 minutes. Physical activity of mice in calorimetric chambers was monitored using infrared laser beam breaks and quantified. Data were recorded for a 24-hour period.

2.16 Thermogenesis study

For non-shivering thermogenesis, mice were fasted at room temperature for four hours and then anesthetized by intraperitoneal injection of ketamine/xylazine/acepromazine (10 mg/kg for ketamine, 2 mg/kg for xylazine, and 1 mg/kg for acepromazine). Rectal core

temperature was measured every 5 minutes after injection for 30 minutes. Mice were sacrificed after the experiment.

2.17 Statistical analysis

All results are presented as mean ± SEM. Statistical analyses were conducted using Excel (Microsoft). For between group comparisons, a two-tailed unpaired Student's t-test was applied. Where appropriate, data were analyzed by ANOVA followed by Fisher's least significant difference (LSD) posthoc test to compare means between groups. P values of < 0.05 were considered significant.

Chapter 3. Results

3.1 IRF2BP2 plays an essential role in macrophage polarization.

Mouse macrophage cells, Raw 264.7, were treated with LPS (100ng/ml) or IL4 (5ng/ml) for 8 hours to induce M1 or M2 phenotype, respectively. Western blotting showed increased IRF2BP2 level in the M2 macrophages, and decreased levels in the M1 cells (Figure 6A).

To investigate if IRF2BP2 plays a role in macrophage polarization, BMDMs cultured from heterozygote (HET, see methods) or IRF2BP2MKO mice. Figure 6B illustrates the ablation of IRF2BP2 in the MKO BMDM, shown with western blotting. BMDM from both groups were treated with LPS (100 ng/ml) or IL-4 (5 ng/ml) for 8 hours to induce M1 or M2 polarization, respectively. BMDM cultured from male and female mice were tested separately. Relative expression of genes known as markers of M1 and M2 were quantified using qPCR on the harvested RNA. IL-1β, TNFα, CCL2 and iNOS were used as markers of the M1 phenotype. As shown in Figure 6C, levels of these M1 markers were increased in male KO BMDMs, demonstrating a more robust M1 phenotype in these cells after treating with LPS. On the other hand, induction of the M2 markers Arginase1, Fizz1, Mgl1 and MRC1 by IL-4 was compromised in male KO BMDMs (Figure 6D). In contrast to male KO BMDMs or female littermate control BMDMs, female KO BMDMs showed a blunted response to LPS (Figure 6E). Similar to male KO BMDMs, female KO BMDMs were also deficient in their response to IL4-induced M2 marker genes (Figure 6F). We also measured IL1-β levels in the conditioned medium of HET and KO BMDMs. KO BMDMs released significantly more IL1-β into the medium under basal culture conditions. When treated with LPS, a similar elevation in IL1-β in the medium was detected but levels were not different

between HET and KO, which might be due to a saturating effect of LPS on IL1-β expression (Figure 6G).

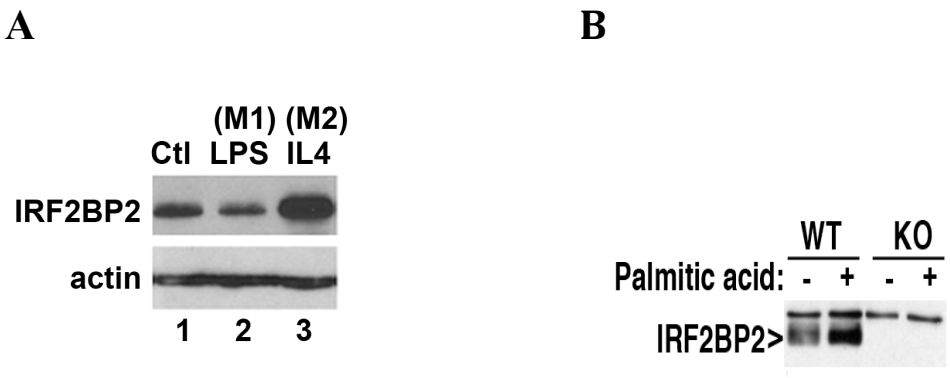
A
(M1) (M2)
Ctl LPS IL4
IRF2BP2
actin
1 2 3
B
WT KO
Palmitic acid: - + - +
IRF2BP2>

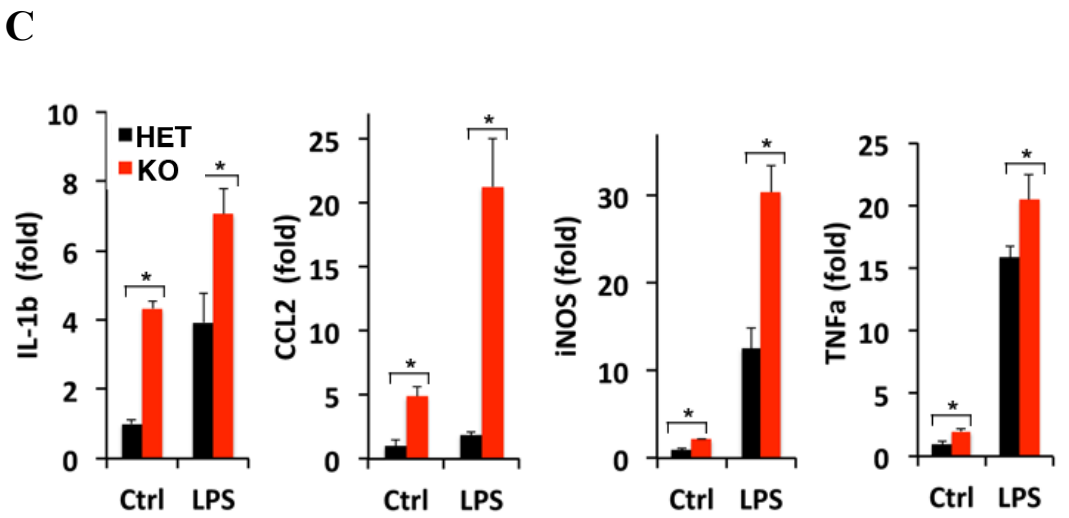
C
HET
KO
IL-1b (fold)
CCL2 (fold)
iNOS (fold)
TNFa (fold)
Ctrl LPS

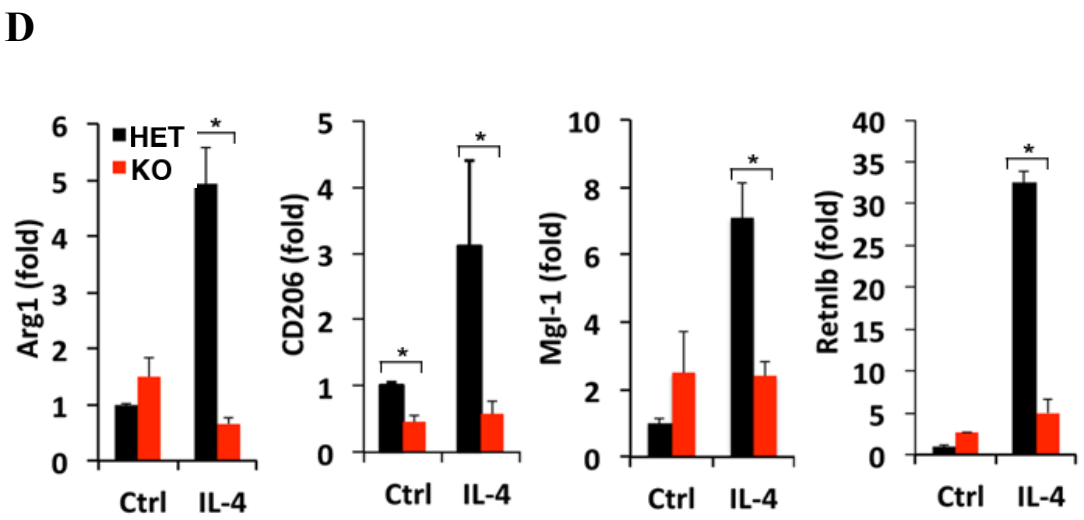
D
HET
KO
Arg1 (fold)
CD206 (fold)
Mgl-1 (fold)
Retnlb (fold)
Ctrl IL-4

E

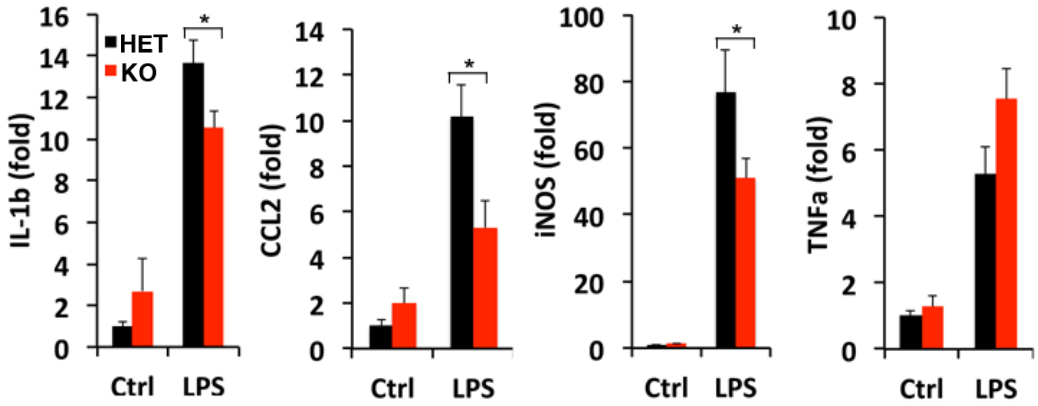
HET
KO
IL-1b (fold)
CCL2 (fold)
iNOS (fold)
TNFa (fold)
Ctrl
LPS

F

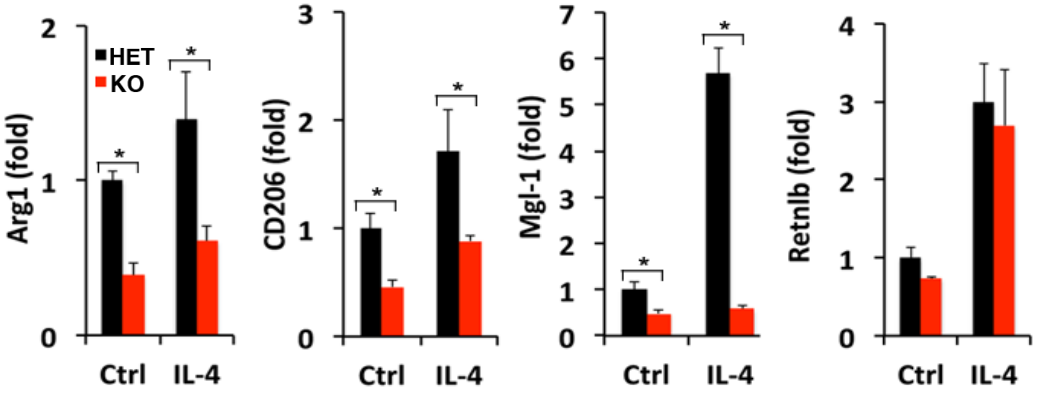
HET
KO
Arg1 (fold)
CD206 (fold)
Mgl-1 (fold)
Retnlb (fold)
Ctrl
IL-4

G

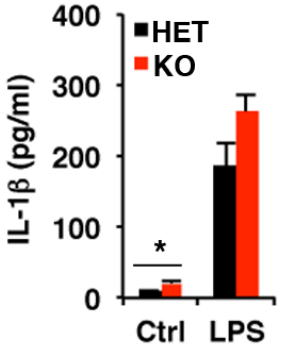
HET
KO
IL-1β (pg/ml)
Ctrl
LPS

Figure 6: Inflammatory function of IRF2BP2 in macrophages. A) Raw 264.7 cells were treated with LPS (100ng/ml) or IL4 (5ng/ml) to induce M1 or M2 phenotype, respectively. Western blot showed increased IRF2BP2 level in the M2 phenotype, and decreased level in the M1 cells. **B)** Western blotting of BMDM protein extract from MKO and control BMDM showing ablation of IRF2BP2 in these cells. **C, D, E, F)** BMDMs cultured from HET or IRF2BP2MKO were induced to M1 or M2 using LPS (100ng/ml) or IL4 (5ng/ml) treatment for 8 hours. Levels of M1 and M2 markers are evaluated using qPCR, n=3 independent cultures. **C)** Relative mRNA expression of M1 markers IL1β, TNFα, CCL2 and iNOS were increased in the **male** KO BMDM. **D)** Expression level of markers of M2, Arginase1, Retnlb (Fizz1), Mgl1 and MRC1 were less induced in the **male** KO cells after treating with IL4. **E)** Unlike male BMDM, M1 markers are less induced in female KO BMDM comparing to HET. **F)** Similar to male BMDM, female KO BMDM are deficient to the induction of M2 markers after IL4 treatment. **G)** BDMD conditioned medium was removed after 8 hours of treatment with LPS or ctrl and IL1-β level was tested with ELISA. KO BMDM release more IL1-β into their conditioned medium. Xun Zhou, one of the lab members, has performed the ELISA. Asterisks indicate $p<0.05$.

3.2 IRF2BP2MKO mice are prone to obesity and glucose intolerance.

Macrophage inflammatory function has been linked to its metabolic function (Lumeng and Saltiel, 2011). Considering the association of genetic variants near IRF2BP2 with increased serum LDL-cholesterol levels, identified in GWAS studies, we speculated that IRF2BP2 might have a role in regulating macrophage metabolic function. Thus, IRF2BP2MKO and their littermate control (LC) mice were fed with a high fat diet (HFD, 60% calories from fat) or chow starting from 6 weeks of age for 28 weeks (male n=12 per group, female n=8 per group). As shown in Figure 7A and 7B, male IRF2BP2MKO gained more weight than LC mice, as early as 13 weeks after HFD feeding. No difference was seen between LC and KO when fed with chow. Interestingly, female mice were resistant to weight

gain with HFD feeding. KO females on a HFD gained less weight than the chow fed female LC mice (Figure 7B).

To investigate if obesity in these mice is associated with its commonly coexisting metabolic phenotype of impaired glucose handling, we performed the Glucose Tolerance Test (GTT). Consistent with their HFD-induced weight gain, male KO mice had impaired glucose handling suggesting that the mice are insulin resistant compared to control male mice (Figure 7C). On the other hand, female KO mice displayed a normal glucose tolerance, consistent with the absence of HFD-induced weight gain compared to female littermate controls.

In order to understand the physiological underpinnings of the weight gain in the MKO mice, we performed metabolic tests to measure their food intake and energy expenditure. Male KO mice showed similar food intake levels to male LC mice after switching from chow to HFD. However, female KO mice had significantly lower levels of food intake when switched to HFD (Figure 7D). These same mice were subjected to calorimetric assessment after 4 weeks on the HFD. Similar energy expenditures were measured between LC and KO male mice, but the respiratory exchange ratio indicated that the male KO mice rely relatively more on carbohydrates as a fuel source than LC male mice (Figure 7E (RER)). Female KO mice on the other hand, burned more energy than the LC mice, as indicated by elevated VO_2 consumption and utilize more fat as an energy source than LC female mice (Respiratory exchange rate (RER) closer to 0.7 indicates fat utilization whereas RER closer to 0.8 indicates carbohydrate as a fuel source). In order to have a better understanding of the time frame in which the energy expenditure changes in female, we repeated the calorimetric experiment on a separate cohort of mice that were fed a HFD for only one week. As it is shown in Figure 7F, no difference is seen between LC and KO mice

in neither male nor female cohorts in the source of fuel they are consuming (RER) after one week on HFD. We also measured the level of heat production over a 24 hour time period, which seemed to be comparable between LC and MKO in male and female mice (Figure 7G). Thus, male and female mice gradually acquire their different metabolic phenotypes in response to 4 weeks of HFD.

To further elucidate the heat production at physiological condition as an important component of energy expenditure, we measured non-shivering thermogenesis in IRF2BP2MKO and LC mice fed HFD for 2 months. Mice were fasted for four hours and then were anesthetized using ketamine/xylazine. Body temperature that was measured every 5 minutes after injection for 30 minutes proved to be similar between LC and KO male and female mice (Figure 7H).

A

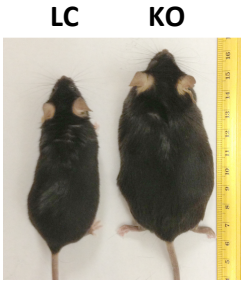
LC
KO

B

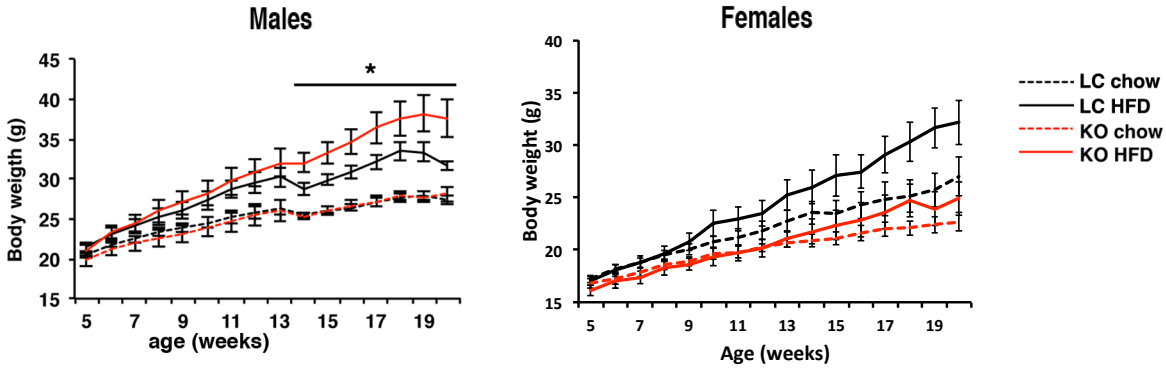
Males
Body weigth (g)
age (weeks)
*
Females
Body weight (g)
Age (weeks)
LC chow
LC HFD
KO chow
KO HFD

C

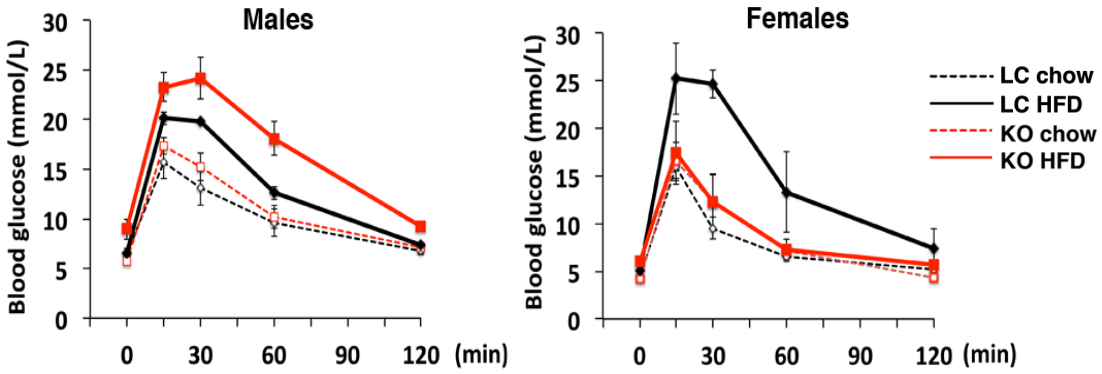
Males
Blood glucose (mmol/L)
(min)
Females
Blood glucose (mmol/L)
(min)
LC chow
LC HFD
KO chow
KO HFD

D

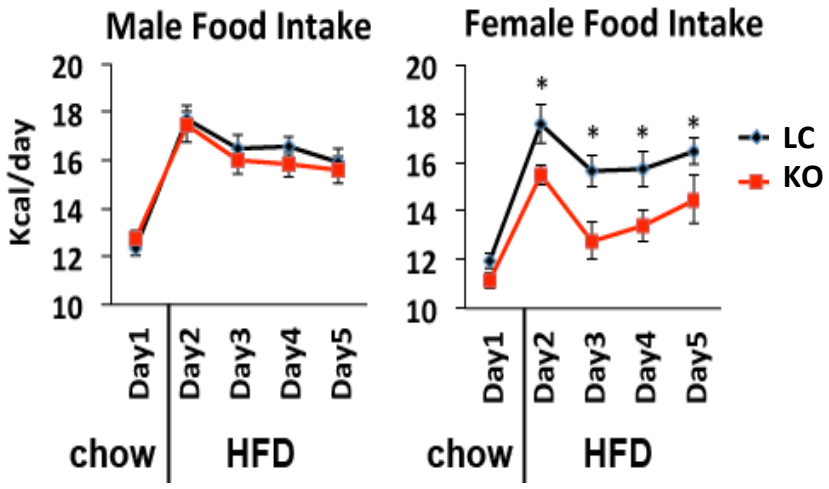
Male Food Intake
Female Food Intake
Kcal/day
20
18
16
14
12
10
Day1
Day2
Day3
Day4
Day5
chow
HFD
LC
KO
*

E

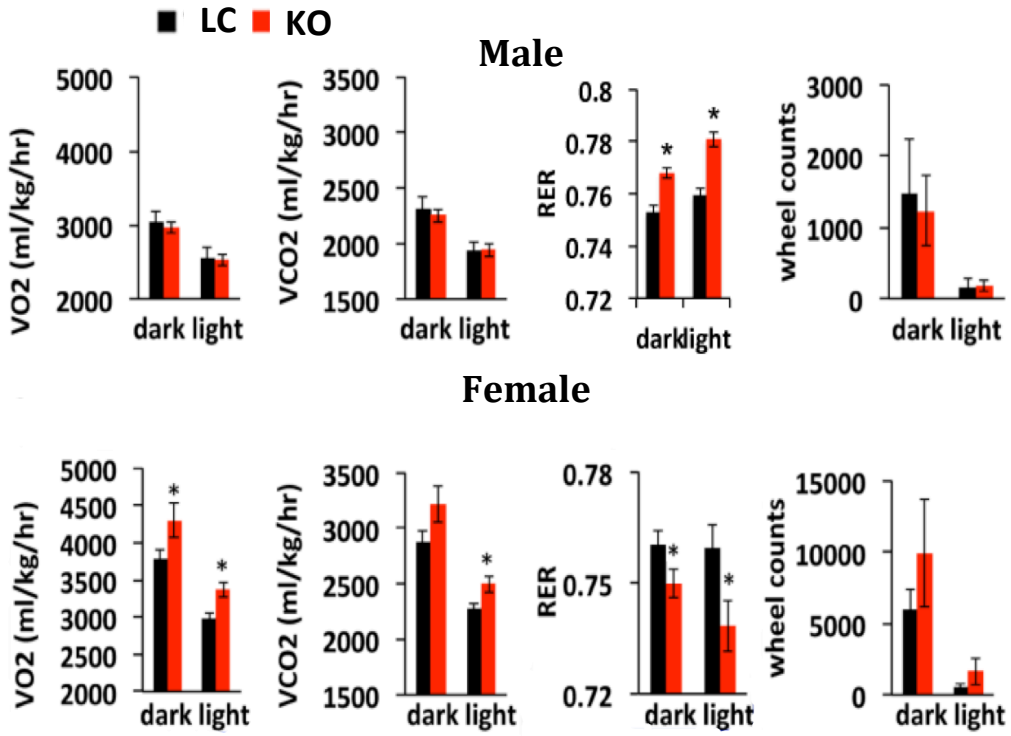
LC
KO
Male
Female
VO2 (ml/kg/hr)
VCO2 (ml/kg/hr)
RER
wheel counts
dark light
darklight
*

F

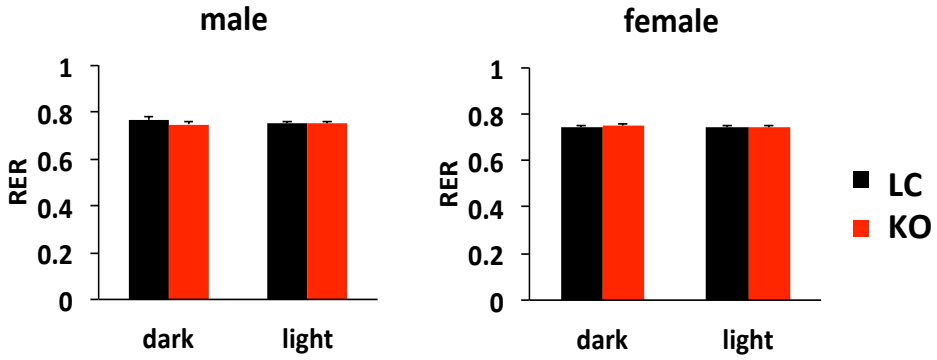
male
female
RER
1
0.8
0.6
0.4
0.2
0
dark
light
LC
KO

G

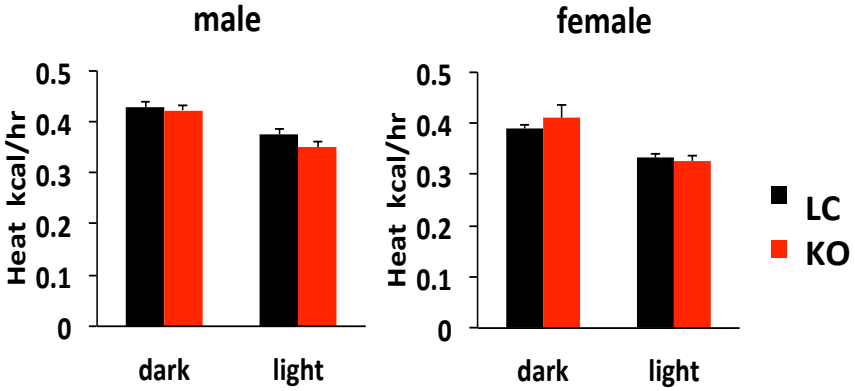
male
female
Heat kcal/hr
0.5
0.4
0.3
0.2
0.1
0
dark
light
LC
KO

H

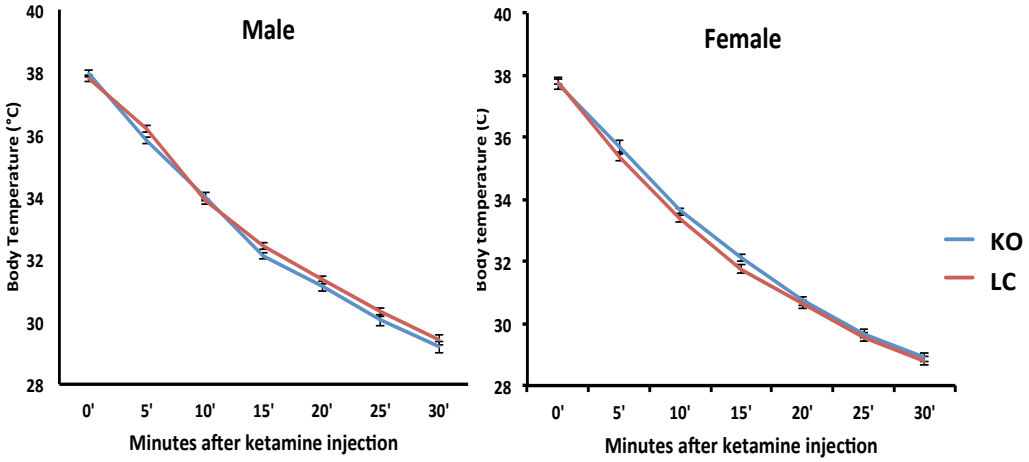
Male
Female
Body Temperature (°C)
Body temperature (C)
40
38
36
34
32
30
28
0'
5'
10'
15'
20'
25'
30'
Minutes after ketamine injection
KO
LC

Figure 7: IRF2BP2MKO male mice show robust obesity and insulin resistance when fed HFD. IRF2BP2MKO or littermate control (LC) mice were fed with HFD or chow starting from 6 weeks old for 28 weeks. **A)** A representative image of a KO mouse compared to a LC, both fed with HFD for 28 weeks. **B)** Two diagrams showing weight gain of four groups of male and four groups of females (male n=12 per group, female n=8 per group). No difference in body weight was detected between WT and HET mice (data not shown) **C)** Glucose Tolerance Test (GTT) of male and female mice (n=3 per group). **D)** Food intake was measured in 24 hour time periods for 5 days. On the second day, mice were switched from chow to HFD. IRF2BP2MKO male mice showed similar food intake level to LC mice after switching from chow to HFD (n=8-11 per group). However, female mice had significantly lower level of food intake when switched to HFD. **E)** Calorimetric experiments were conducted on single-housed mice that were fed with HFD for 4 weeks before starting the tests. The results demonstrated similar energy expenditure between LC and IRF2BP2MKO in male mice with the MKO consuming relatively more carbohydrates than LC (RER). Female MKO mice on the other hand, burn more energy than the LC, and tend to burn relatively more fat than LC (n=8-11 per group). **F)** Calorimetric experiments were repeated for mice that have been on HFD only for one week. No difference is seen between LC and IRF2BP2MKO mice in neither male nor female cohorts in regards to their RER value (n=12 per group). **G)** We also measured the level of heat production over a 24 hour time period, which seemed to be comparable between LC and MKO in male and female mice (n=8-11 per group). **H)** To measure non-shivering thermogenesis, mice were fasted for four hours and then were anesthetized using ketamine/xylazine. Body temperature that was measured every 5 minutes after injection for 30 minutes proved to be similar between LC and KO male and female mice that were fed HFD for 2 months (n=8-10 per group). All experiments in this figure have been done in collaboration with Xun Zhou. Asterisks indicate $p<0.05$.

3.3 Systemic inflammation and hepatic steatosis in HFD fed IRF2BP2MKO male mice.

Obesity is often associated with hepatic steatosis or fatty liver, which is characterized by liver inflammation and fat accumulation in the liver. Considering the fact that resident macrophages of the liver also known as Kupffer cells play an important role in the

development of steatosis (Rivera et al., 2007), we examined the liver pathology in the HET and KO HFD fed mice (Figure 8A&B). Histology analysis of liver from HFD-fed male IRF2BP2MKO mice showed a remarkable steatosis compared to HFD-fed male HET mice, as indicated by oil-red-O staining of large neutral lipid droplets. Astonishingly, HFD-fed IRF2BP2MKO females had less steatosis than littermate HET female mice fed the same diet (Figure 8A).

Systemic inflammation is the major phenotype of IRF2BP2MKO male mice. It is evident by macrophage infiltration in the different tissues such as liver, white adipose tissue (WAT) and spleen as shown in Figure 8B, C and D; and even aorta (Figure 11A). F4/80 is used to stain all macrophages and Kupffer cells in the liver. CD68 is another pan-macrophage marker, which we used to stain macrophages in WAT. Inducible nitric oxide synthase (iNOS) is a marker of inflammation and iNOS staining revealed extensive M1 activation of macrophages in the liver and WAT (Figure 8B and 8C). Hemosiderin-laden macrophages were also abundant in the spleen of the male KO mice (Figure 8D). Female mice on the other hand did not show macrophage infiltration in their liver, WAT or spleen.

QPCR results presented in Figure 6B showed that male KO BMDMs have a higher expression of IL1-β, even under basal conditions. Since elevated IL1-β secretion is a hallmark of systemic inflammation, we sought to check the level of this cytokine in the HET and IRF2BP2MKO mice serum. We found a trend of increased IL1-β level in male KO serum (Figure 8E).

A

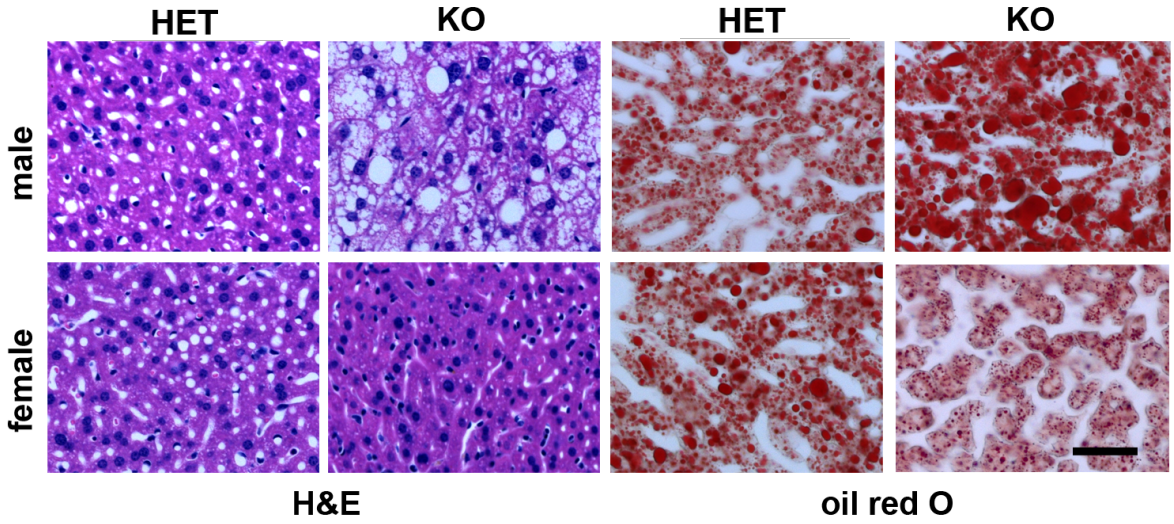
HET
KO
HET
KO
male
female
H&E
oil red O

B

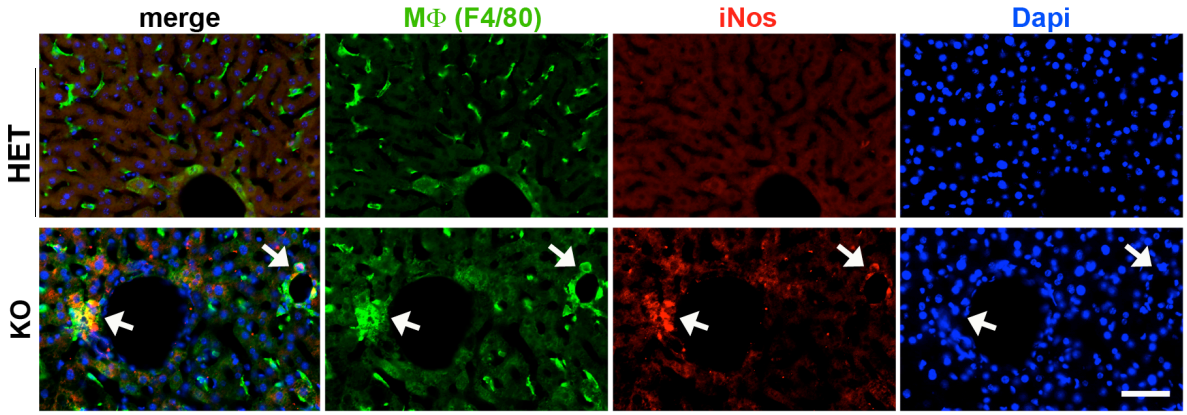
merge
MΦ (F4/80)
iNos
Dapi
HET
KO

C

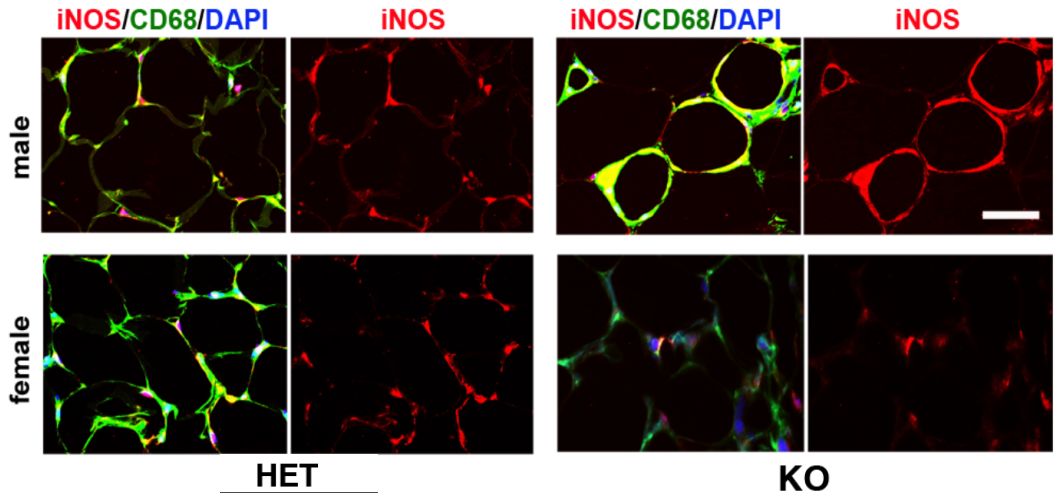
iNOS/CD68/DAPI
iNOS
iNOS/CD68/DAPI
iNOS
male
female
HET
KO

D

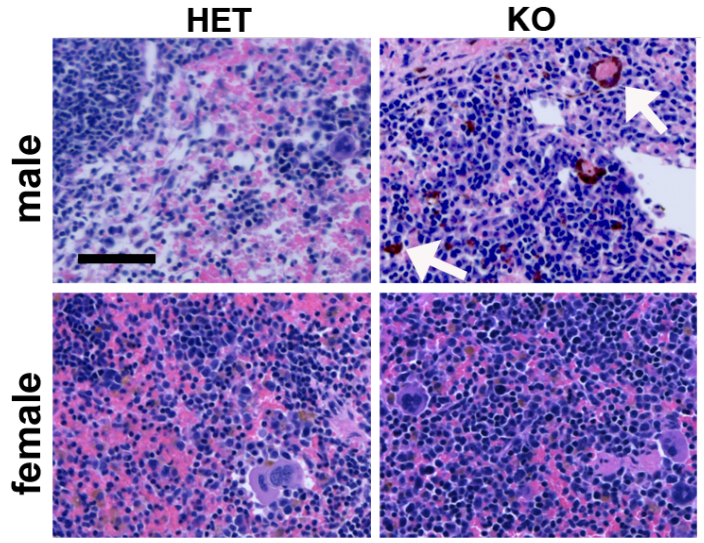
HET
KO
male
female

E

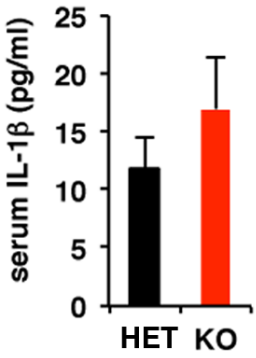

Figure 8: IRF2BP2MKO mice have more severe hepatic steatosis, as well as systemic inflammation in peripheral organs when fed HFD. **A)** Liver H&E staining (left) and oil-red-O staining (right) of HET and KO mice. Scale bar = 50 um. **B)** Immunofluorescence staining of liver tissue, arrows: macrophages. F4/80 and iNOS were used as markers of total macrophages and M1 macrophages, respectively. **C)** Immunofluorescence staining of WAT. CD68 and iNOS were used as markers of total macrophages and M1 macrophages, respectively. Scale bar = 50 um. **D)** H&E staining of spleen, arrows: hemosiderin-laden macrophages. Scale bar = 50 um. **E**) Serum IL1β level was measured by ELISA (HET n=4, KO n=5). ELISA is performed by Xun Zhou.

3.4 Cholesterol and lipoprotein metabolism is affected in IRF2BP2MKO mice.

Serum cholesterol was measured in HET and KO mice after 20 weeks feeding with HFD or chow. We observed increased total serum cholesterol in the KO (Figure 9A). To have a better understanding of the cholesterol metabolism in these mice, we performed Fast Protein Liquid Chromatography (FPLC). After 5 months of HFD, mice were fasted overnight (16 hours) and serum samples were pooled from 3 male mice in each group. Serum samples were used to measure the lipoprotein profile by FPLC for chow-fed and for HFD-fed IRF2BP2MKO and HET mice, in collaboration with Dr. Katey Rayner of the University of

Ottawa Heart Institute. Fractions were aligned according to the position of the serum albumin peak measured by densitometry and total cholesterol was measured for each fraction. The identity of the peaks was confirmed by immunoblot of the FPLC fractions using anti-mouse ApoB (a generous gift of Dr. Ross Milne of the University of Ottawa Heart Institute) and anti-mouse ApoA1 antibodies. Although little difference was observed in the lipoprotein profile between chow fed IRF2BP2MKO and littermate control mice (Figure 9B), profiles were markedly different after a HFD. LDL-C that was increased in littermate control mice and was even more so in male IRF2BP2MKO mice. In addition, the IDL peak was elevated in the male IRF2BP2MKO mice. In the male HFD group there was also a striking increase in the HDL peak in the MKO mice, which may be an important factor in the atherosclerosis total risk equation. Note that ApoE levels were higher in HET male mice fed a HFD than in IRF2BP2MKO male mice (Figure 9B).

HFD increased VLDL cholesterol in female littermate control mice but not in female IRF2BP2MKO mice. Otherwise, female HET and IRF2BP2MKO mice have similar levels of lipoproteins (Figure 9C).

It is also noteworthy that the level of ApoE expression in the serum of IRF2BP2MKO female mice on HFD is significantly higher than HET female mice on HFD (Figure 9C).

A

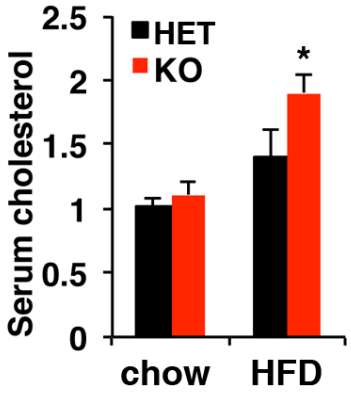
HET
KO
*
Serum cholesterol
2.5
2
1.5
1
0.5
0
chow
HFD

B

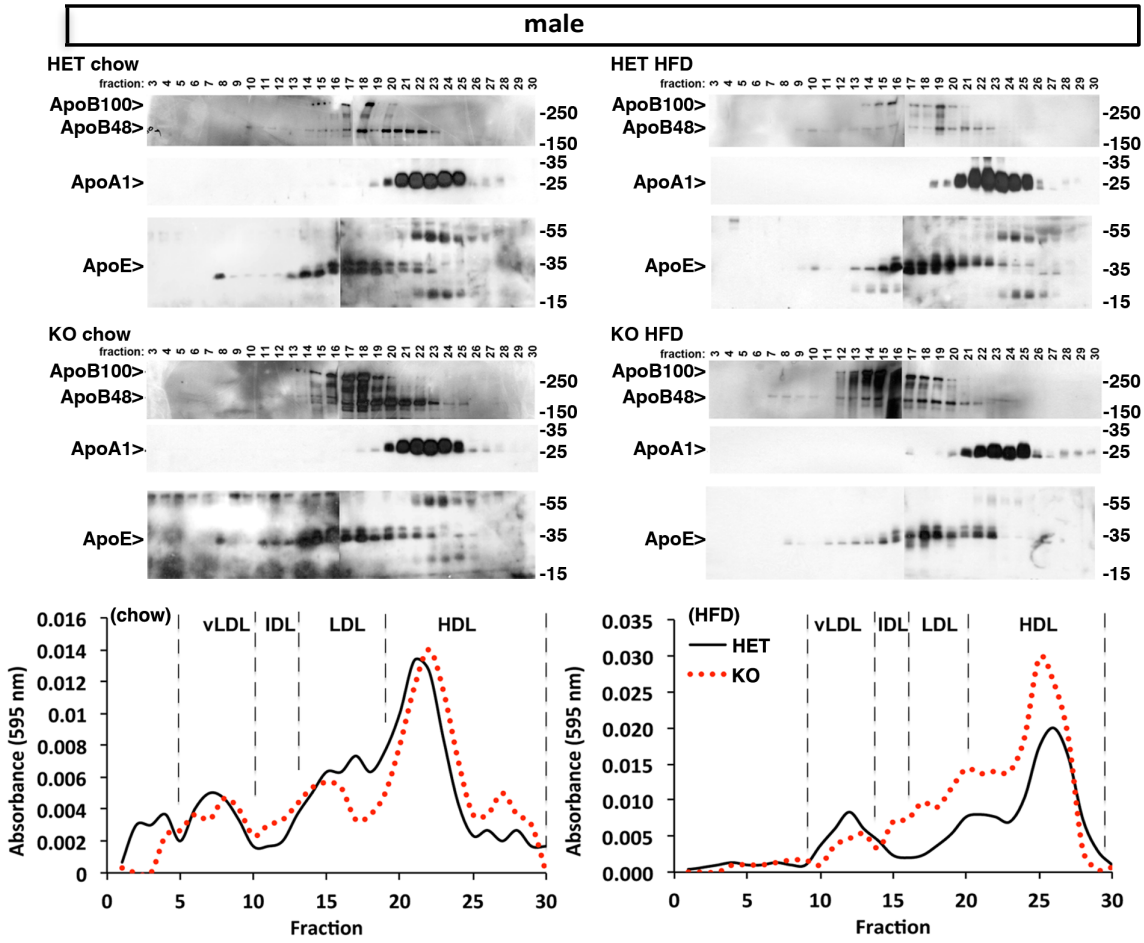
male
HET chow
HET HFD
KO chow
KO HFD
fraction:
ApoB100>
ApoB48>
ApoA1>
ApoE>
-250
-150
-35
-25
-55
-35
-15
(chow)
(HFD)
HET
KO
vLDL
IDL
LDL
HDL
Absorbance (595 nm)
Fraction

C

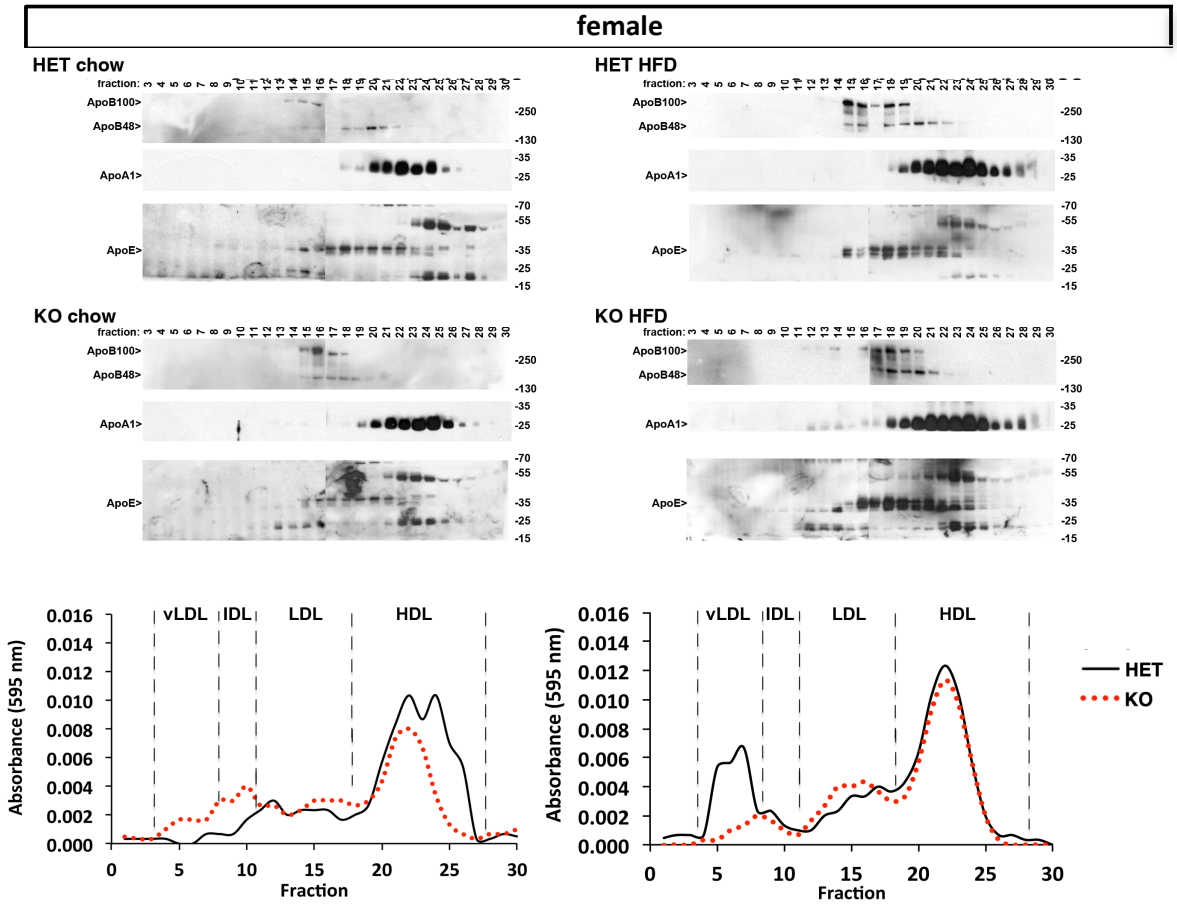

Figure 9: Cholesterol metabolism in altered in IRF2BP2MKO mice. A) Serum cholesterol was measured in HET and KO male mice after 20 weeks on HFD or chow (n=3 per group). **B, C)** Fast Protein Liquid Chromatography (FPLC) on male (B) and female serum (C). Each sample is composed of equal amount of serum pooled from 3 mice. FPLC is conducted in Dr. Katey Rayner in Heart Institute. All western blottings are done by Dr. Nihar Pandey.

3.5 Ablation of IRF2BP2 in macrophages alters macrophage cholesterol metabolism.

To have a better understanding of the role of IRF2BP2 in cholesterol metabolism at cellular level, we treated BMDM from HET and IRF2BP2MKO with oxLDL 30 μg/ml and tested the macrophage cholesterol uptake changes as well as changes in IRF2BP2 expression level. As shown in Figure 10A, IRF2BP2 protein and mRNA level is increased after 24 hours of oxLDL treatment.

Cholesterol uptake was quantified by treating BMDM with ^{3}H-cholesterol containing AcLDL (see methods). IRF2BP2MKO BMDM took up significantly more AcLDL than the HET cells (Figure 10B). There was increased oxLDL accumulation in the KO BMDM after 48 hours of treatment, shown with oil-red-O staining in Figure 10C. Total and free cholesterol were both higher in MKO BMDM compared to littermate control after AcLDL loading. However, the ratio of esterified to free cholesterol was not different, indicating that cholesterol storage and mobilization are not impaired in MKO BMDM (Figure 10D). The increased free cholesterol would be expected to be toxic and pro-inflammatory (Li et al., 2005).

Cholesterol efflux in HET and KO BMDM was quantified after 48 hours of ^{3}H-cholesterol pre-treatment followed by HDL or ApoA1 treatment. Both male and female BMDM showed lower cholesterol efflux comparing to their corresponding HET cells (Figure 10E).

Excessive cholesterol loading has been shown to affect macrophage inflammatory state. Since IRF2BP2MKO macrophages have more pro-inflammatory characteristics, we used IL1-β, a pro-inflammatory cytokine as an indicator of macrophage activation state after oxLDL treatment. As shown in Figure 10F, oxLDL induces IL1-β secretion in both HET and KO BMDM, although the KO level of IL1-β secretion is higher than the HET.

QPCR analysis of ApoE mRNA detected lower expression of this gene in the BMDMs of IRF2BP2MKO mice compared to controls (Figure 10G). Since macrophages synthesize ApoE, the ability to efflux cholesterol in the absence of an apolipoprotein acceptor measures "autocrine" ApoE-dependent efflux.

A

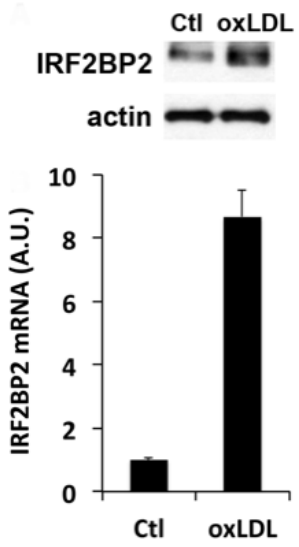
Ctl
oxLDL
IRF2BP2
actin
IRF2BP2 mRNA (A.U.)
10
8
6
4
2
0
Ctl
oxLDL

B

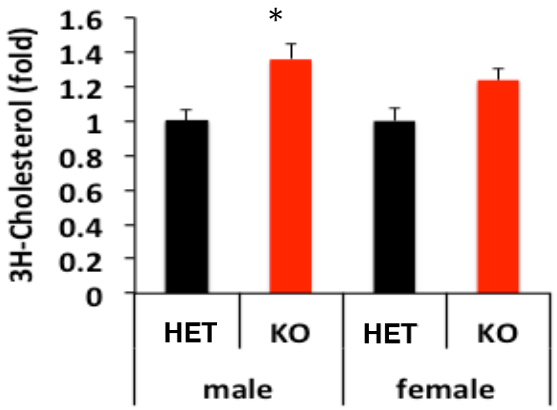
3H-Cholesterol (fold)
1.6
1.4
1.2
1
0.8
0.6
0.4
0.2
0
*
HET
KO
HET
KO
male
female

C

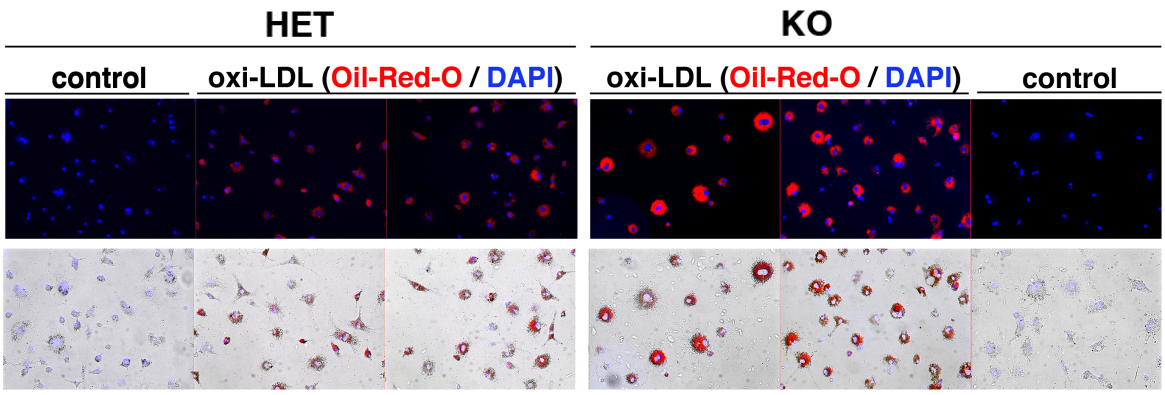
HET
KO
control
oxi-LDL (Oil-Red-O / DAPI)
oxi-LDL (Oil-Red-O / DAPI)
control

D

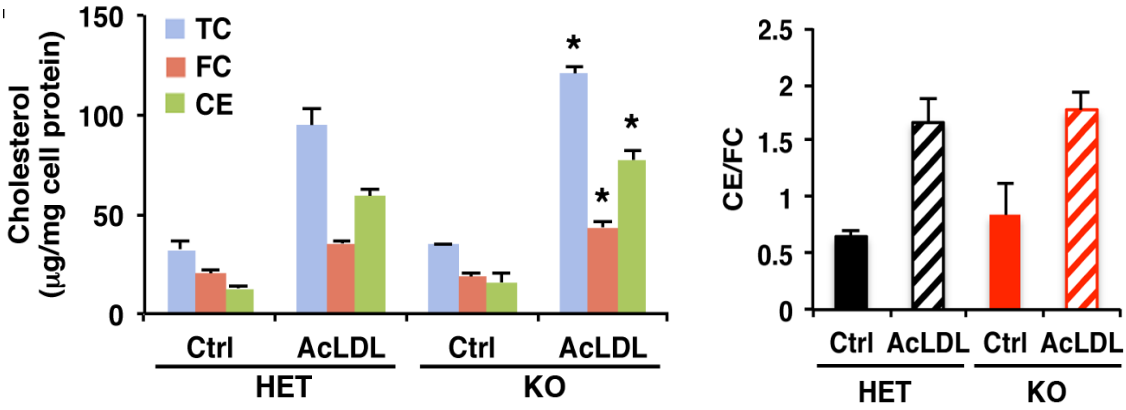
Cholesterol (µg/mg cell protein)
150
100
50
0
TC
FC
CE
*
*
*
Ctrl
AcLDL
Ctrl
AcLDL
HET
KO
CE/FC
2.5
2
1.5
1
0.5
0
Ctrl
AcLDL
Ctrl
AcLDL
HET
KO

E

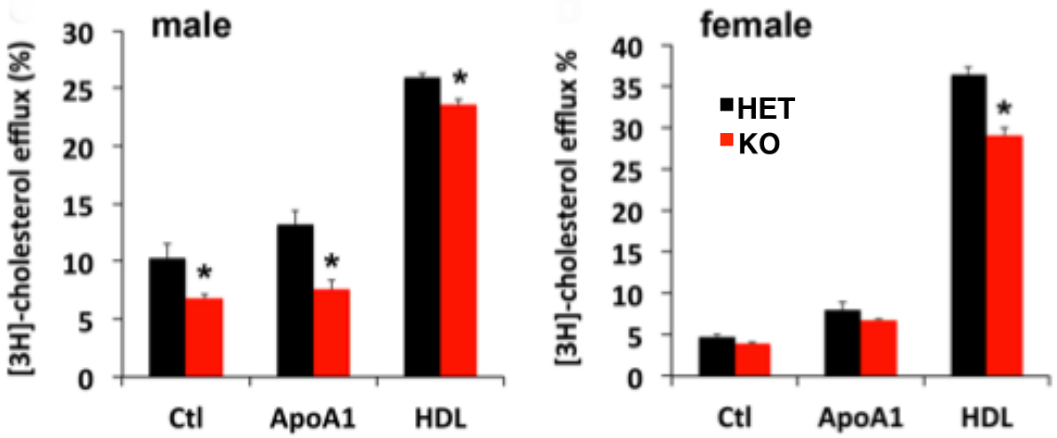
male
[3H]-cholesterol efflux (%)
30
25
20
15
10
5
0
*
*
*
Ctl
ApoA1
HDL
female
[3H]-cholesterol efflux %
40
35
30
25
20
15
10
5
0
HET
KO
*
Ctl
ApoA1
HDL

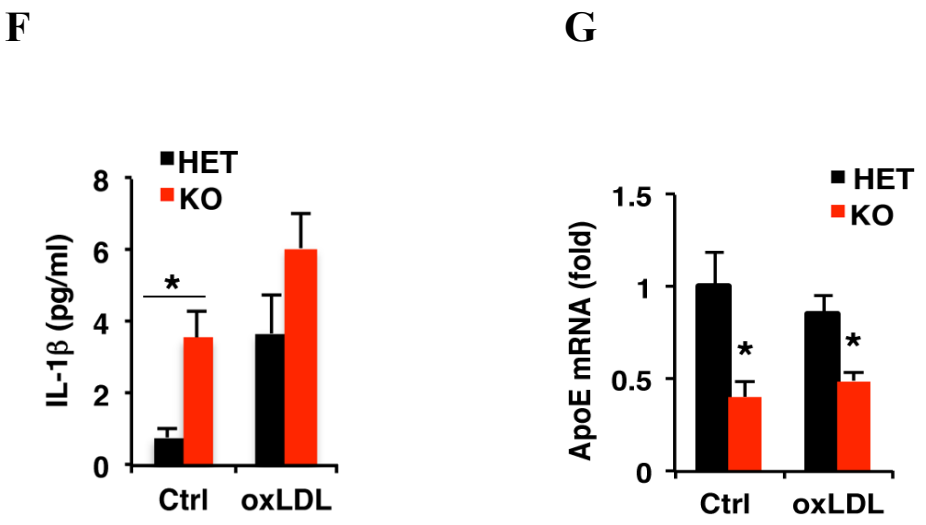

Figure 10: Metabolic function of IRF2BP2 in macrophages. A) BMDM from HET and KO were treated with oxLDL 30µg/ml for 24 hours. Using western blotting and real-time PCR, IRF2BP2 protein and mRNA level is demonstrated to be increased after oxLDL treatment. **B)** Oil-red-O staining of the HET and IRF2BP2KO BMDM, after treating with control or oxLDL for 48 hours. **C)** Cholesterol uptake measured after 30 minutes treatment of HET and IRF2BP2MKO BMDM from male or female mice with 3H-Cholesterol containing AcLDL (50µg/ml). **D)** Cholesterol content of HET and IRF2BP2MKO BMDM treated with control or AcLDL (50µg/ml) for 24 hours. **E)** Cholesterol efflux in HET and KO BMDM was quantified after treating the cells with 3H-cholesterol for 48 hours and then inducing cholesterol efflux by HDL or ApoA1. **F)** BMDM from HET and KO was treated with control or oxLDL 30µg/µl for 48 hours. IL1-β secretion in the media was quantified using ELISA. **G)** Quantitative PCR analysis of ApoE mRNA from HET and IRF2BP2MKO BMMDM demonstrating lower ApoE expression from MKO cells. N=3 independent cultures, asterisks indicate $p<0.05$. IL1-β ELISA is conducted by Xun Zhou.

3.6 IRF2BP2MKO bone marrow transplantation to LDLR-/- mice reduces atherogenesis.

As it was discussed in Figure 8, systemic inflammation is the major phenotype of IRF2BP2MKO mice that were fed HFD. We observed hemosiderin-laden macrophages in the cusps of aortic roots in those mice. Immunofluorescence staining with macrophage specific antibody, F4/80, confirmed the macrophage infiltration in the aortic valve (Figure 11A).

In order to investigate the role of IRF2BP2MKO macrophages in the process of atherosclerosis, we performed bone marrow transplantation from IRF2BP2MKO or HET mice to LDLR-/- mice (MKO→LDLR-/- and HET→LDLR-/-, respectively). The mice were recovered for 6 weeks and then were fed with western diet for 12 weeks. Aortic valves were dissected and sectioned to quantify the lesion area (see methods). Interestingly, the MKO→LDLR-/- mice were demonstrated to have similar extent of atherosclerosis to HET→LDLR-/-; studied with H&E and oil-red-O staining (Figure 11B).

We further studied the valves with immunofluorescence staining for macrophage pro- and anti-inflammatory markers. Both groups of valves showed to have abundant macrophage infiltration, with more pro-inflammatory phenotype (Figure 11C).

Ablation of IRF2BP2 augments the level of apoptosis in different cell types e.g. neurons (our lab, data not shown), breast cancer cells (Tinnikov et al., 2009) and osteosarcoma cells (Koeppel et al., 2009). It also has been shown that enhanced apoptosis in macrophages contributes to a decreased atherosclerotic lesion size (Arai et al., 2005; Babaev et al., 2008). Therefore, we assessed the extent of apoptosis in the lesion areas of our HET and IRF2BP2MKO transplanted animals. As it is shown in Figure 11C and 11D, TUNEL staining and Caspase 3 staining revealed that MKO→LDLR-/- transplanted mice have

increased apoptotic areas than the HET→LDLR-/- animals. We also evaluated the level of apoptosis in vitro in cultured BMDM. As shown in Figure 11E, apoptosis is increased in the MKO cells especially after oxLDL treatment.

Another remarkable observation was the hypertrophy of heart muscle in the MKO→LDLR-/- animals relative to HET→LDLR-/- mice (Figure 11F). The interventricular septum showed significant hypertrophy and this is often a clinical sign of aortic stenosis (Kansal et al., 1979). It remains to be determined whether MKO→LDLR-/- mice have more significant aortic valve calcification, which could account for more severe septal hypertrophy in these mice. This can be also due to the systemic inflammation in the MKO transplanted mice (Miguel-Carrasco et al., 2010) or a consequence of higher level of hypercholesterolemia in these mice (Kang et al., 2009).

A

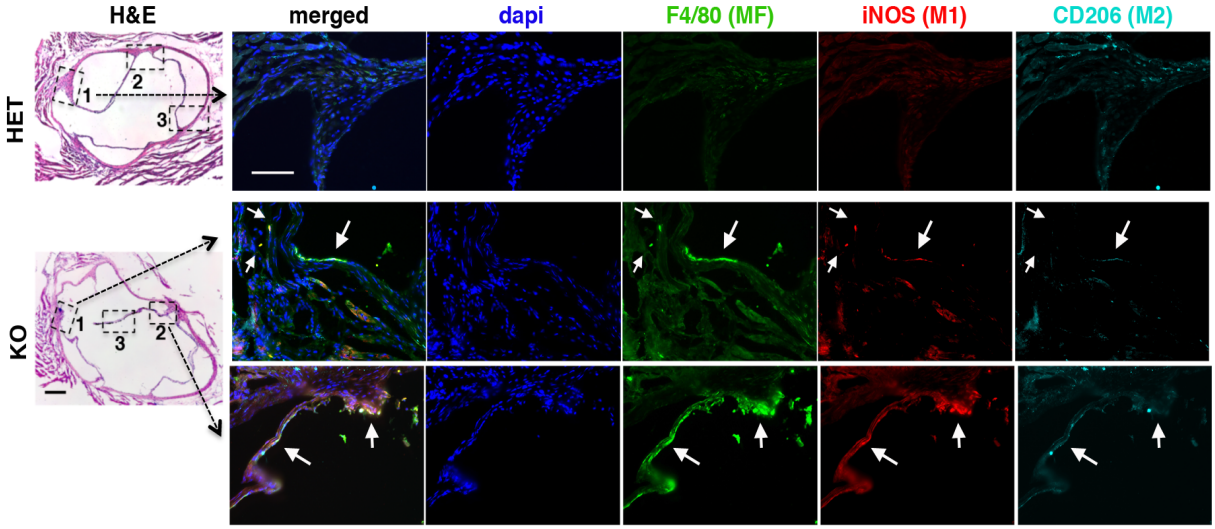
H&E
merged
dapi
F4/80 (MF)
iNOS (M1)
CD206 (M2)
HET
KO
1
2
3

B

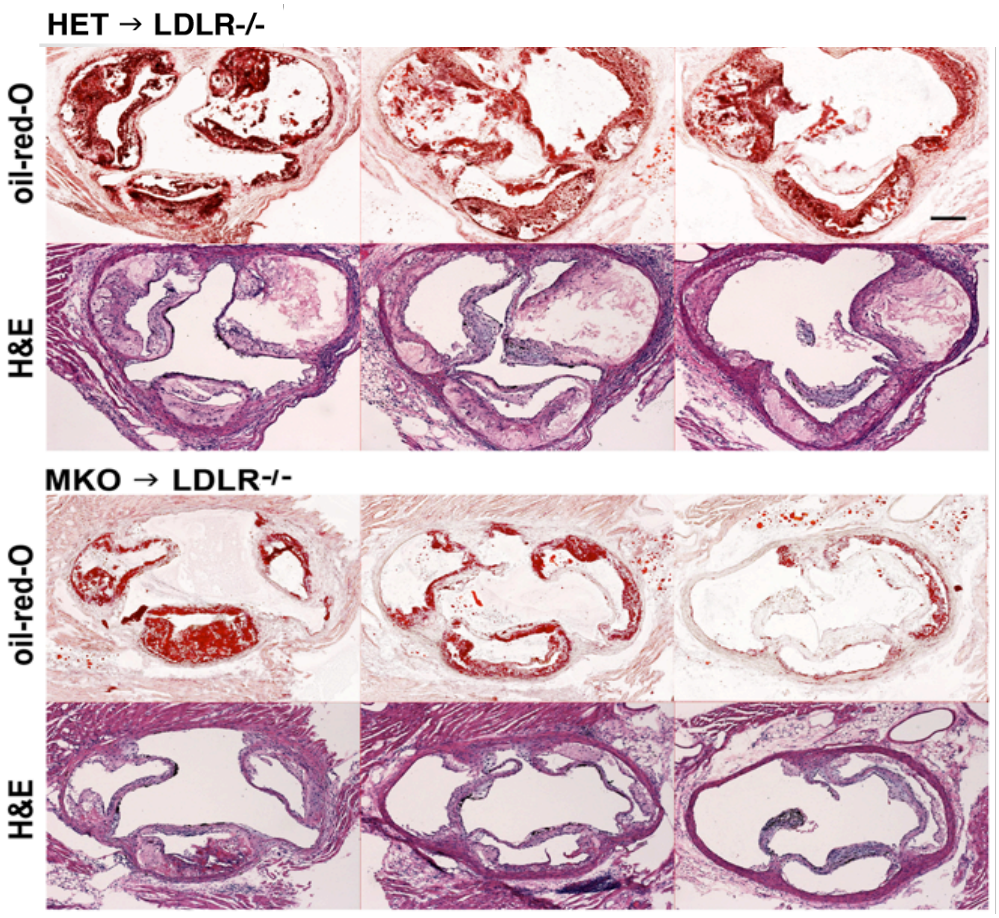
HET → LDLR-/-
oil-red-O
H&E
MKO → LDLR-/-
oil-red-O
H&E

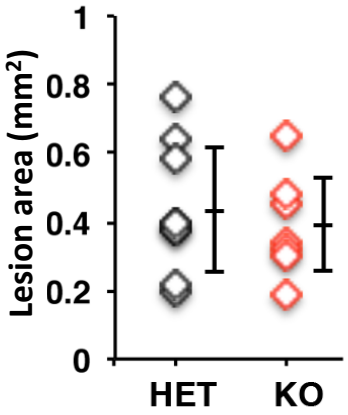
Lesion area (mm²)
1
0.8
0.6
0.4
0.2
0
HET
KO

C

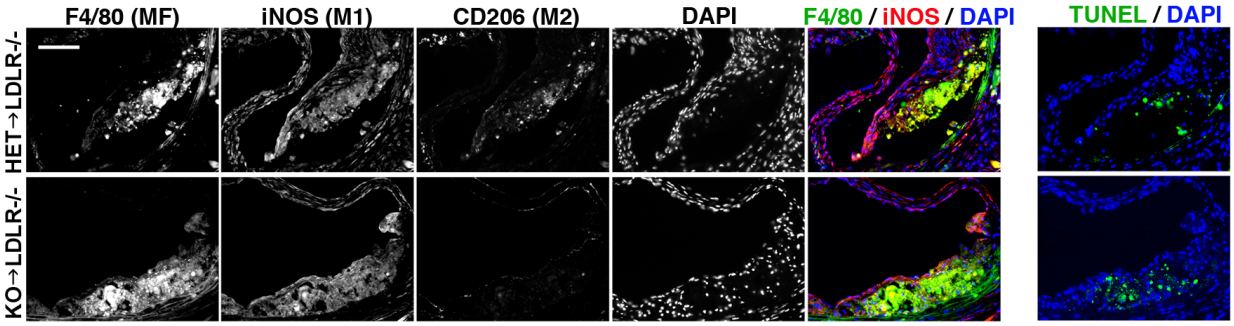
F4/80 (MF)
iNOS (M1)
CD206 (M2)
DAPI
F4/80 / iNOS / DAPI
TUNEL / DAPI
HET→LDLR-/-
KO→LDLR-/-

D

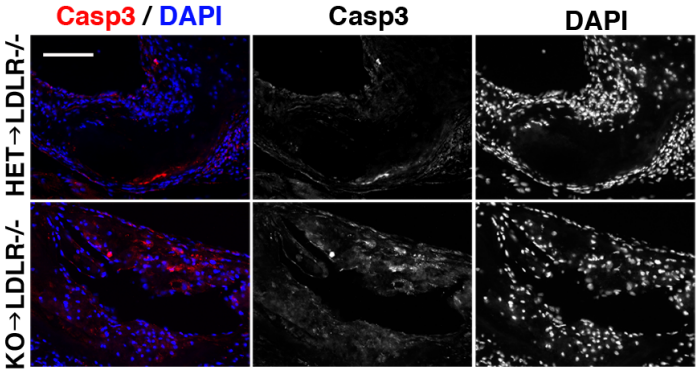
Casp3 / DAPI
Casp3
DAPI
HET→LDLR-/-
KO→LDLR-/-

E

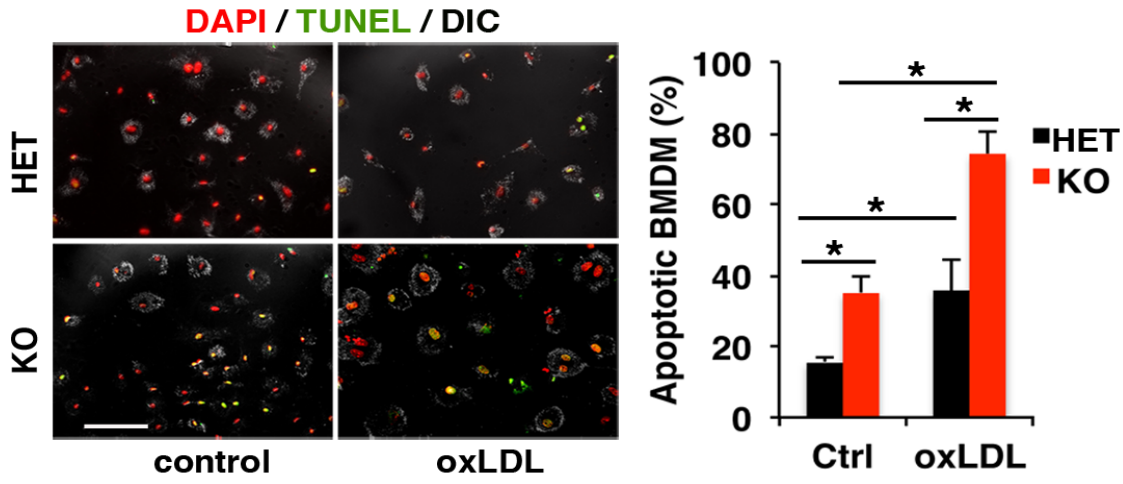

F

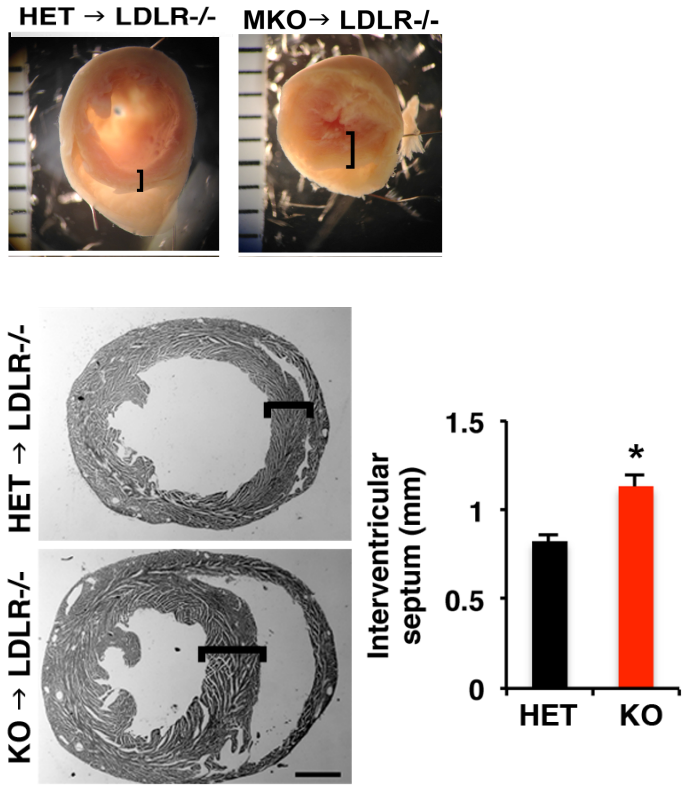

Figure 11: MKO bone marrow transplantation to LDLR-/- mice reduces atherosclerosis lesion size partly due to increased apoptosis. A) Immunofluorescence staining of aortic root in HET or IRF2BP2MKO mice.

Arrows: macrophages. F4/80, iNOS and CD206 were used as markers of total macrophages, M1 macrophages, M2 macrophages, respectively. Scale bar: 200 μm. **B)** Aortic valves (10μm thickness) from LDLR-/- mice transplanted with HET or IRF2BP2MKO mice after feeding with western diet for 12 weeks. Valve sections are stained with H&E or oil-red-O and the lesion areas were quantified as Mean ± Standard Deviation. N= 9 HET, 8 KO. **C)** Immunofluorescence staining of valve sections. F4/80, iNOS and CD206 were used as markers of total macrophages, M1 macrophages, M2 macrophages, respectively. TUNEL staining of aortic sections shows increased apoptotic cells within the plaques of MKO→LDLR-/- mice. TUNEL staining is done by Xun Zhou. Scale bar: 100 μm. **D)** Increased activated caspase 3 (Casp3) within the plaques of KO→LDLR-/- mice. Scale bar: 100 μm. **E)** In vitro TUNEL staining of cultured BMDM treated with oxLDL. Quantification of apoptotic cells shows enhanced level of apoptosis in MKO BMDM, especially after oxLDL treatment. N=7 fields each from BMDM of 2 HET and 2 KO mice. Scale bar: 100 μm. **F)** Cardiac hypertrophy in the LDLR-/- mice transplanted with IRF2BP2MKO bone marrow. Interventricular septum thickness was higher in MKO→LDLR-/- mice comparing to HET→LDLR-/- mice. Cardiac muscle histology (12μm thickness) and quantification of the difference between interventricular septum thickness in MKO→LDLR-/- mice comparing to HET→LDLR-/-, (n=6 per group), Scale bar: 1mm. Asterisks indicate $p<0.05$.

3.7 Transcription of metabolic regulatory genes is altered in IRF2BP2MKO BMDM.

In order to recognize the main players affected by IRF2BP2, we performed microarray on WT and KO BMDM RNA. Findings are summarized in Table 2 and Table 3 for male and female BMDM respectively. Microarray results of the male BMDM confirmed by real-time PCR and western blotting are presented in Figure 12. As shown in Table 2 and Table 3, expression of IRF2BP2 is 5-10 fold decreased in the MKO microarrays but not completely eliminated. This is partly due to the fact that RNA is isolated from primary culture of BMDM, which may contain residual cells other than myeloid lineage, e.g. fibroblasts. Although we performed analysis of the expression of inflammatory and

metabolic genes for both male and female mice, I will focus on our results from male mice in this report.

We tested whether the expression of scavenger receptors responsible for uptake of oxLDL were altered in KO macrophages. Although we found no change in the mRNA expression of CD36 and scavenger receptor B1, LOX1 was more than 50 percent higher in KO BMDMs (Figure 12A). CD36 protein levels were higher in the KO BMDM, which can be due to altered post-transcriptional regulation of CD36 (Figure 12D).

Among genes that are linked to cholesterol efflux, ABCA9 transcription was lower to less than a half of its normal expression. But no significant change was seen in ABCA1 or ABCG1 (Figure 12B) mRNA levels.

Expression profiling of male KO BMDM revealed strikingly reduced expression of **Sort1**, a key vacuolar protein in hepatocytes controlling plasma LDL-C. In addition, the transcription factor **Klf2**, a key suppressor of monocyte pro-inflammatory cytokine expression was also markedly reduced in male KO BMDM (Figure 12C, 12D).

We sought to further investigate the role of IRF2BP2 in regulating transcriptional level of KLF2, which itself is a transcription factor that suppresses inflammatory gene expression in macrophages. Klf2 expression is dependent on the transcription factor MEF2 (Kumar et al., 2005). Our lab identified IRF2BP2 as an interacting partner of Vgll4 and TEAD4 (Teng et al., 2010), transcription factors that our lab also showed interact with MEF2 (Maeda et al., 2002; Chen et al., 2004). Thus, we predict that IRF2BP2 works through the Mef2 regulatory sequence to activate high levels of KLF2 expression in BMDM.

Therefore, our lab generated wild type and MEF2 binding site mutant KLF2 promoter luciferase reporters and tested the effect of IRF2BP2 knockdown and over-expression on KLF2 promoter activity. As shown in Figure 12E, knockdown of IRF2BP2 in F11 cells

decreases the luciferase activity of wild type KLF2 reporter while it has no effect on the mutant reporter with the mutated MEF2 binding site. IRF2BP2 overexpression on the other hand, increased the wild type KLF2 reporter activity but not the mutant reporter activity. This confirms the IRF2BP2 as the regulator of KLF2 expression in a MEF2 dependent manner.

A

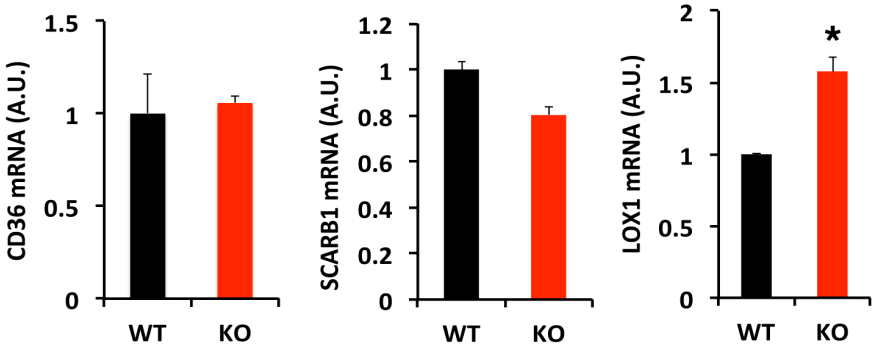
CD36 mRNA (A.U.)
1.5
1
0.5
0
WT
KO
SCARB1 mRNA (A.U.)
1.2
1
0.8
0.6
0.4
0.2
0
WT
KO
LOX1 mRNA (A.U.)
2
1.5
1
0.5
0
*
WT
KO

B

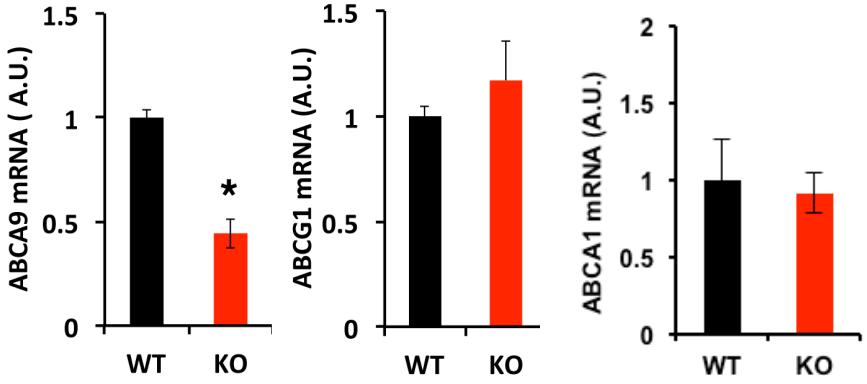
ABCA9 mRNA (A.U.)
1.5
1
0.5
0
*
WT
KO
ABCG1 mRNA (A.U.)
1.5
1
0.5
0
WT
KO
ABCA1 mRNA (A.U.)
2
1.5
1
0.5
0
WT
KO

C

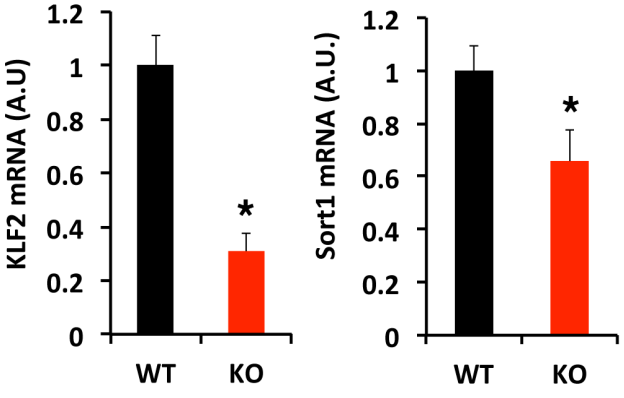
KLF2 mRNA (A.U)
1.2
1
0.8
0.6
0.4
0.2
0
*
WT
KO
Sort1 mRNA (A.U.)
1.2
1
0.8
0.6
0.4
0.2
0
*
WT
KO

D

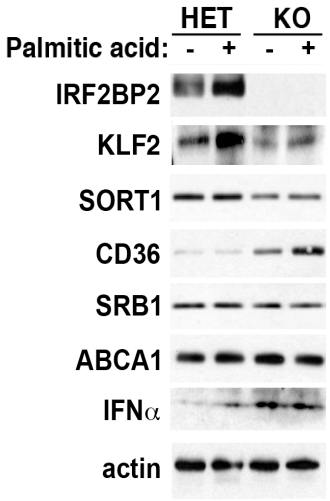
HET
KO
Palmitic acid: - + - +
IRF2BP2
KLF2
SORT1
CD36
SRB1
ABCA1
IFNα
actin

E

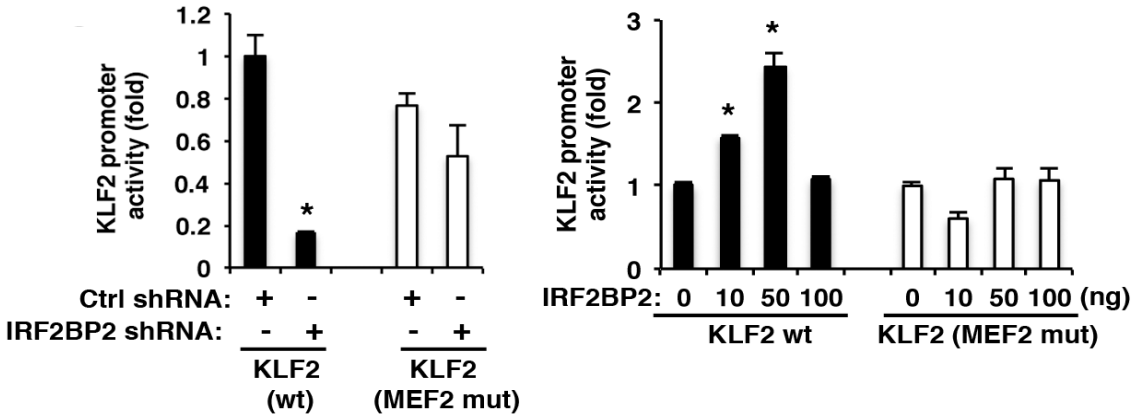

F

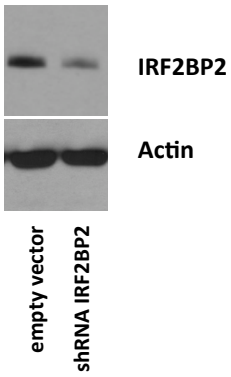

Figure 12: Expression of metabolic regulatory genes is altered in IRF2BP2MKO male BMDM. A, B, C) Transcriptional expression level of several genes in littermate control (WT) and IRF2BP2MKO, tested by qPCR. N= 3 cultured BMDM from individual mice per group. **D)** Western blotting of protein levels in HET and IRF2BP2MKO BMDM after palmitic acid (400 μM in 0.8 mN NaOH) treatment for 6 hours. Western blotting is perfomed by Dr. Nihar Pandey. **E)** Knockdown of IRF2BP2 in F11 cells decreases the luciferase activity of wild type KLF2 reporter while it has no effect on the mutant reporter with the mutated MEF2 binding site. IRF2BP2 overexpression on the other hand, increased the wild type KLF2 reporter activity but not for the mutant one. Mean ± standard deviation. N=4 wells each. Asterisks indicate $p<0.05$. KLF2 promoter assay is performed by Xun Zhou. **F)** Western blotting confirms IRF2BP2 knockdown using shRNA IRF2BP2 in F11 cells.

Table 2: Selected transcripts whose expression is altered in male IRF2BP2MKO macrophages. M1 markers are in red. Independent student t-test is used to analyze the data.

Gene Symbol	KO/WT	WT avg ± SD	KO avg ± SD	ttest	M1/M2 marker
Irf2bp2	0.1	631 ± 25	94 ± 9	4.1E-06	M2
Inflammatory cytokines					
Il1a	0.6	187 ± 6	105 ± 6	7.9E-05	M1
Il1b	3.2	140 ± 12	454 ± 106	7.0E-03	M1
Il17ra	1.8	214 ± 14	387 ± 50	4.6E-03	M2
Il10	1.8	349 ± 135	643 ±104	4.1E-02	M2
Tnf	1.3	1336 ± 102	1788 ± 103	5.6E-03	M1
Ccl3 (MIP-1α)	1.1	4203 ± 82	4772 ± 56	5.8E-04	M1
Ccl4 (MIP-1β)	1.9	354 ± 44	670 ± 35	6.1E-04	M1
Ccl12	3.0	52 ± 9	155 ± 20	1.2E-03	M1
Ccl7	2.2	553 ± 118	1223 ± 179	5.7E-03	M1
Ccl8	2.6	83 ± 23	220 ± 38	5.8E-03	M1
Ccl6	0.8	1935 ± 33	1562 ±116	5.9E-03	M2
Ccl2 (MCP-1)	1.8	1104 ± 105	1994 ± 360	1.5E-02	M1
Cxcr3	0.8	95 ± 4	72 ± 3	1.1E-03	-
Ccr3	1.6	127 ± 15	204 ± 6	1.2E-03	M1
Genes of Interest					
FOLR2	0.3	1473 ± 197	375 ± 47	7.2E-04	M2
Klf2	0.6	176 ± 13	112 ± 6	1.3E-03	M2
Itga9	2.1	253 ± 68	532 ± 24	2.5E-03	-
Sort1	0.6	516 ± 58	321 ± 30	6.8E-03	M2
Irf2bpl (EAP1)	1.6	163 ± 11	267 ± 41	1.3E-02	-
ZDHHC14	0.7	469 ± 20	310 ± 9	2.3E-04	M2
C-type lectin domain family					
Mrc1	0.5	711 ± 41	330 ± 41	3.4E-04	M2
Olr1	1.7	33 ± 2	56 ± 7	4.9E-03	M1
Clec12a	1.1	1973 ± 3	2218 ±40	4.4E-04	-
Clec7a	1.5	392 ± 48	602 ± 40	4.3E-03	M2
Clec4n	0.6	684 ± 89	415 ± 47	9.8E-03	-
Clec10a	0.5	51 ± 8	28 ± 5	1.6E-02	M2
NLR domain family					
Naip6	0.8	378 ± 29	284 ± 5	5.5E-03	-
Naip1	0.8	89 ± 4	68 ± 6	8.2E-03	-
Naip5	0.7	402 ± 41	299 ± 15	1.5E-02	-
Naip2	0.9	884 ± 49	766 ± 46	3.7E-02	-
Nlrp1b	0.8	79 ± 7	61 ± 4	2.3E-02	-
Nlrc4	0.8	219 ± 15	181 ± 133	3.1E-02	-
LDL receptor related proteins					
Ldlrad3	0.7	837 ± 72	569 ± 16	3.3E-03	M2
Lrp12	0.8	976 ± 62	759 ± 44	7.8E-03	M2
Lrp8	1.2	154 ± 8	186 ± 9	1.2E-02	M1
ATP-binding cassette transporters					
Abca9	0.6	152 ± 20	88 ± 6	6.4E-03	M2
Abca6	0.8	15 ± 1	12 ± 1	7.6E-03	-
Abcc3	0.8	909 ± 65	683 ± 49	8.4E-03	M2
Abcd2	0.6	158 ± 13	100 ± 17	8.8E-03	M2
Matrix metallopeptidases					
Mmp19	0.6	642 ± 6	415 ± 15	1.9E-05	M2
Mmp2	2.1	119 ± 23	245 ± 2	6.4E-04	M1

Table 3: Selected transcripts whose expression is altered in female IRF2BP2MKO macrophages. Genes whose expression was regulated in opposite directions in male and female IRF2BP2MKO mice are shown in blue. Genes that were altered in male IRF2BP2MKO but showed no significant change in female IRF2BP2MKO were shown in grey. Independent student t-test is used to analyze the data.

female					
Gene Symbol	KO/WT	WT avg ± SD	KO avg ± SD	ttest	M1/M2 marker
Irf2bp2	**0.2**	**437 ±124**	**83 ± 20**	**8.16E-03**	**M2**
Klf2	**0.7**	**134 ± 38**	**99 ± 40**	**1.96E-02**	**M2**
snord15b	**0.7**	**162 ± 13**	**110 ± 23**	**2.80E-02**	
snora73b	**0.7**	**225 ± 18**	**167 ± 30**	**4.82E-02**	
Gdf3	**1.7**	**88 ± 11**	**152 ± 6**	**8.06E-04**	
Inflammatory cytokines					
Il1a	1.2	141 ± 39	170 ± 160	7.77E-01	M1
Il1b	2.8	205 ± 61	566 ± 344	1.49E-01	M1
Il17ra	**1.6**	**215 ± 15**	**342 ± 62**	**2.65E-02**	**M2**
Il10	**1.4**	**460 ± 108**	**651 ± 76**	**6.68E-02**	**M2**
Tnf	1.4	1585 ± 185	2275 ± 845	2.39E-01	M1
Ccl3 (MIP-1α)	1.1	3591 ± 129	3819 ± 232	2.12E-01	M1
Ccl4 (MIP-1β)	1.8	430 ±79	789 ± 432	2.30E-01	M1
Ccl12	1.9	77 ± 20	144 ± 83	1.11E-01	M1
Ccl7	1.7	810 ± 273	1352 ± 473	1.61E-01	M1
Ccl8	1.8	105 ±57	184 ± 74	2.20E-01	M1
Ccl2 (MCP-1)	1.4	1326 ± 202	1809 ± 468	1.81E-01	M1
Cxcr3	1.0	69 ± 6	66 ± 3	5.11E-01	-
Ccr3	1.3	113 ± 23	144 ± 33	2.54E-01	M1
other gene					
FOLR2	**0.4**	**903 ± 224**	**349 ± 74**	**1.54E-02**	**M2**

3.8 LXR and PPARγ response is deficient in IRF2BP2MKO BMDM.

As shown in Figure 12, the level of ABCA1 and ABCG1 are not different in the HET and MKO BMDMs under basal conditions. Here we further examined the level of these two receptors with their expression is induced by modified LDL, by an LXR agonist, or by a PPARγ agonist. Interestingly, ABCA1 induction by LXR and PPARγ agonist is impaired in the MKO BMDM (Figure 13). This might contribute to the reduced efflux seen in IRF2BP2MKO macrophages.

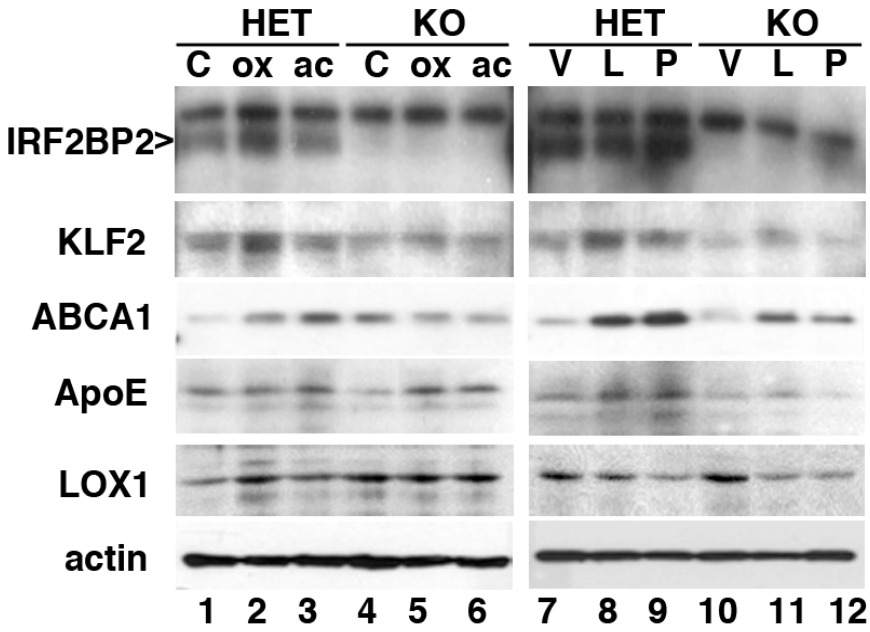

Figure 13: LXR and PPARγ response is impaired in MKO BMDM. Left panel, littermate HET or IRF2BP2MKO BMDM were exposed to control medium (c), medium loaded with oxLDL (ox) or AcLDL (ac), 50 μg/ml for 24 hours. In the right panel, BMDM were treated with the DMSO vehicle (V), with LXR agonist T0901317 (T) (10 μM) or PPARγ agonist, rosiglitazone (Ro) (10 μM) for 24 hours. In MKO BMDM, induction of ABCA1 protein level increase with modified LDL particles is inhibited. Also, LXR and PPARγ effect is diminished on the level of ABCA1. Western blotting was performed by Dr. Nihar Pandey.

Chapter 4. Discussion

New lines of evidence suggest an unexpected overlap between inflammatory and metabolic sensors that elicits a similar tissue response to these two sets of stimulators (Lumeng and Saltiel, 2011). This overlap justifies considering obesity as an inflammatory state. Our results emphasize the effect of systemic inflammation on metabolic pathologies, and highlight the role of macrophages in this process. In this study we demonstrated the role of IRF2BP2 in macrophage polarization, obesity, macrophage cholesterol metabolism and atherosclerosis. When fed a HFD, IRF2BP2MKO male mice showed symptoms consistent with some of the important components of metabolic syndrome including obesity, glucose intolerance and dyslipidemia.

4.1 Anti-inflammatory function of IRF2BP2 in macrophages.

IRF2BP2 expression is dynamically regulated in macrophages: polarization to the inflammatory M1 phenotype suppressed, whereas polarization to the anti-inflammatory M2 phenotype elevated IRF2BP2 expression. Microarray analysis revealed a skewed M1 over M2 marker gene expression in male IRF2BP2MKO BMDMs (Table 2). Of note, culture of BMDM in L929 conditioned medium (containing M-CSF) for 6 days maintains macrophages in an M2 polarized state (Verreck et al., 2004; Verreck et al., 2006). Nonetheless, expression of several well-known M2 markers was profoundly suppressed in male IRF2BP2MKO BMDM, including the folate receptor Folr2 (Puig-Kroger et al., 2009) and the mannose receptor Mrc1 (Odegaard et al., 2008; Fleetwood et al., 2009), whereas inflammatory cytokines like IL1-β (Il1b), TNFα and many CCL chemokine family members were elevated, including CCl2 (MCP-1) (see Table 2). Importantly, qPCR analysis independently confirmed

that ablation of IRF2BP2 in male macrophages promoted the M1 phenotype but hindered M2 marker activation.

In contrast to male BMDM, female MKO Macrophages did not express elevated inflammatory cytokines or CCL chemokines under basal conditions (Table 2) and had a blunted response to LPS-stimulation (Figure 6D).

Of note, since primary BMDM are cultured in vitro for one week without addition of sex hormones, the differences in gene expression profiled by the microarray and by the qRT-PCR analyses reflect intrinsic differences between male and female bone marrow stem cells that may be programmed *in vivo* by sex hormones at the time of isolation. Others have also reported sex-specific intrinsic differences in gene expression retained in cultured BMDM (Bhasin et al., 2008), although the mechanisms that underlie this phenomenon are not known. Because IL-10 suppresses TNFα expression, it is generally considered as an M2 anti-inflammatory marker (Bhargava and Lee, 2012). However, it is important to note that IL-10 can take on a pro-inflammatory phenotype in macrophages primed with interferon alpha (IFNα) (Sharif et al., 2004). Indeed, IRF2BP2MKO macrophages had elevated IFNα expression (see Table 2) and this would convert IL-10 to a pro-inflammatory cytokine.

IRF2BP2 has been shown to directly bind to two transcription factors that regulate inflammatory cytokine expression, IRF2 and NFAT1 (Childs and Goodbourn, 2003) and (Carneiro et al., 2011). Here, we demonstrated the inflammatory function of IRF2BP2 for the first time. However, the exact pathway through which IRF2BP2 controls inflammatory cytokines expression in macrophages is not known. Based on our microarray and qPCR data, we suggest a number of possible mechanistic pathways, and bring some results supporting at least one of the mechanisms.

For instance, an NFκB/NFAT binding sequence in the IL1-β promoter constitutively suppresses IL1-β expression (Lebedeva and Singh, 1997). By binding to and inhibiting NFAT, IRF2BP2 may inhibit IL1-β expression (Diagram 1).

Microarray analysis of IRF2BP2MKO BMDM (Table 2) revealed reduced expression of transcription factor KLF2. Immunoblot analysis also confirmed reduced protein expression (Figure 12D). IRF2BP2 is a co-activator of Vgll4 and Tead4 (Teng et al., 2010; Teng et al., 2011) that promote transcription factor MEF2 activity (Maeda et al., 2002; Chen et al., 2004). MEF2 is a key transcription factor in macrophages that maintains the expression of transcription factor KLF2. As mentioned in introduction chapter, KLF2 inhibits NFκB and AP-1 transcription activity and inhibits the expression of pro-inflammatory genes (Das et al., 2006). Here, we showed that indeed, IRF2BP2 regulates the expression of KLF2 prompter in a MEF2-dependent manner. KLF2 promoter activity was reduced in presence of IRF2BP2 shRNA, and dose-dependently increased when co-transfected with IRF2BP2 overexpression vector. This effect is not seen when we used a KLF2 promoter with a mutant MEF2 binding site (Figure 12E). Thus, ablating IRF2BP2 in macrophages may increase IL1-β expression, reduce expression of Klf2, and thereby activate a host of inflammatory cytokines.

In addition, our data indicate reduced expression of Sort1 in IRF2BP2MKO macrophages. IRF2BP2 likely relieves the inhibitory effect of ATF3 (Kimura, 2008), enabling Sort1 expression. Loss of IRF2BP2 would lead to constitutive suppression of Sort1 expression (see Diagram 1).

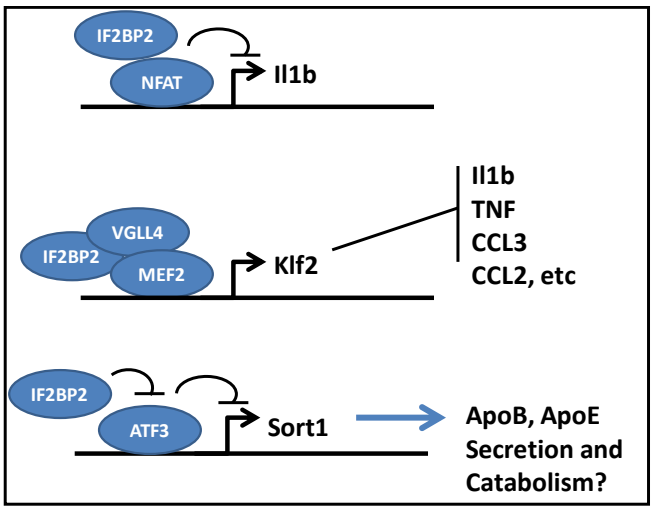

Diagram 1. Proposed model illustrating how IRF2BP2 can suppress transcription of IL1-β (Il1b) yet promote transcription of Klf2 and Sort1.

4.2 Metabolic function of IRF2BP2 in macrophages.

Our study is the first to report a metabolic role for IRF2BP2, contributing in cholesterol homeostasis in macrophages. We showed that IRF2BP2 ablation increases macrophage cholesterol uptake and reduces cholesterol efflux. Cholesterol uptake is the first step toward foam cell formation. Excessive cholesterol accumulation in the cell, especially in the form of free cholesterol, leads not only to the crystal formation and activation of inflammasome, it also interferes with normal ER function and ultimately makes apoptosis inevitable (Moore et al., 2013). We found increased CD36 protein level as well as increased LOX1 mRNA level that are possible routes for the increase in cholesterol uptake. Although CD36 is established as one of the key receptors for macrophage cholesterol uptake with pro-atherogenic characteristics, specific role of macrophage LOX1 in is not studied in progression of atherosclerosis. In endothelial cells however, up-regulation of LOX1 has a pro-atherogenic effect (White et al., 2011).

Efflux to ApoA1 reflects ABCA1-mediated cholesterol transport (Lawn et al., 1999; Singaraja et al., 2009) whereas efflux to HDL reflects ABCG1-mediated cholesterol transport (Kennedy et al., 2005). However, we did not observe reduced ABCA1 total protein levels in BMDM of IRF2BP2MKO mice (Figure 12D), although proper localization of ABCA1 at cell membranes requires palmitoylation (Singaraja et al., 2009) and is influenced by CD36 levels (Yue et al., 2010), and this process may be defective in IRF2BP2MKO BMDM. Since ABCA1 expression is elevated in response to the cholesterol metabolite-sensitive transcription factor LXR (Castrillo et al., 2003) and also PPARγ (Chinetti et al., 2001), reduced efflux can also be attributed to impaired LXR signaling. Indeed, a markedly attenuated activation of ABCA1 was observed in MKO BMDM in response to synthetic LXR (T0901317) or PPARγ (rosiglitazone) ligands. Thus, loss of IRF2BP2 impairs these signaling pathways.

One of the pathways involved in cholesterol efflux, as discussed in the introduction chapter, involves efflux of cholesterol packaged in endogenous ApoE. Since ApoE expression is regulated by LXR signaling (Laffitte et al., 2001), this observation suggests that LXR signaling may be impaired in IRF2BP2-deficient Macrophages. We showed a decrease in ApoE mRNA expression in IRF2BP2MKO BMDM (Figure 10G). This effect could account at least partly for the decrease in efflux in MKO cells. In addition, IRF2BP2 is required for genes putatively controlling cholesterol efflux (Sort1, ABCA9). Inflammatory cytokines increased in IRF2BP2MKO would suppress ABCA1 and ABCG1 palmitoylation, also interfering with cholesterol efflux.

4.3 Systemic phenotype of IRF2BP2MKO mice.

Macrophage-specific ablation of IRF2BP2 renders male mice more susceptible to high fat diet-induced obesity (Figure 7B) and impaired glucose homeostasis (Figure 7C). In contrast, female IRF2BP2MKO mice are protected from these phenotypes (Figure 7B, C). In obesity, macrophages infiltrate adipose tissue causing increased inflammation (Weisberg et al., 2003) and promoting insulin resistance associated with adiposity (Kanda et al., 2006). Thus, in HFD fed IRF2BP2MKO mice, where higher serum IL1-β levels indicate a stronger inflammatory response, increased adiposity and impaired insulin response appear to be a viscous cycle. Profound hepatic steatosis in the KO is also a consequence of this hyper-inflammatory state. Histological analysis of liver, spleen and aorta also confirmed the increased macrophage activation in the IRF2BP2MKO tissues.

We were also surprised by the altered lipoprotein profile of IRF2BP2MKO mice, since hepatocytes rather than macrophages are considered to be the primary regulators of serum lipoproteins and cholesterol homeostasis (Raffai et al., 2003). Our result suggests macrophages, or perhaps the Kupffer cells in IRF2BP2MKO male mice can influence hepatic cholesterol homeostasis, accounting for the observed lipoprotein profile. Histological studies show that for every 4 hepatocytes there is 1 Kupffer cell in the mouse liver (Lopez et al., 2011). Kupffer cells influence hepatocyte fatty acid oxidation (Odegaard et al., 2008). Of note, CCL-2 (MCP-1) produced by macrophages was shown to decrease lipid uptake and cholesterol efflux to ApoA1 in HepG2 cells (Huang et al., 2013). So, cytokines produced by macrophages can disrupt hepatic control of lipoproteins and cholesterol indirectly.

We were also intrigued by the increased IDL. IDL particles come from VLDL that have lost most of their triglyceride, but retain cholesteryl esters. IDL particles are

distinguished by their content of multiple copies of ApoE, in addition to a single copy of ApoB100, that allow IDL to bind to the LDL receptor with a very high affinity. Further triglyceride hydrolysis converts IDL to LDL and the ApoE leaves the particle and only the ApoB-100 remains. Thereafter, the affinity for the LDL receptor is much reduced (Brown and Goldstein, 1986). Of note, ApoE deficiency in humans results in an accumulation of plasma IDL, and decreased LDL, consistent with a block in the conversion of IDL to LDL (Gabelli et al., 1986).

Systemic infiltration of macrophages in the male IRF2BP2MKO mice was striking. We discovered presence of more macrophages in adipose tissue, liver, spleen and aortic valve. In MKO mice, infiltration of macrophages with brown pigments in H&E staining was evident, most probably with features of hemosiderin-laden macrophages. More tests need to be done to identify the nature of pigments and their origin (Figure 8D, white arrows).

Infiltration of macrophages in the cusps of aortic valve was manifested in male IRF2BP2MKO mice fed with HFD for 6 months. This was consistent with our data regarding the increase in the expression of CCL-2 in the MKO BMDM in vitro. CCL-2 is a strong chemokine attracting macrophages. Its role in atherosclerosis has been confirmed with the studies that reported decrease in atherogenesis by ablating CCL-2 or its receptor, CCR-2 (Boring et al., 1998; Gu et al., 1998). In another study, over-expression of CCL-2 in adipose tissue led to infiltration of macrophages in adipose tissue, insulin resistance and hepatic steatosis (Kanda et al., 2006).

To clarify the role of macrophage IRF2BP2 in atherogenesis process, we transplanted bone marrow from male IRF2BP2MKO mice to male LDLR-/- mice. They were fed western diet for 12 weeks before sacrificing. Studying their aortic valves revealed that overall area affected with atherosclerosis is not different than HET→LDLR-/- mice. Although it was a

surprising result, further studies showed that there is more apoptosis in the lesions of MKO→LDLR-/- mice. As discussed earlier, a number of studies demonstrated that increasing the level of apoptosis in macrophages leads to a strong anti-atherogenic effect (Arai et al., 2005; Liu et al., 2005; Babaev et al., 2008). More apoptosis in macrophages inhibits early lesion development most probably by terminating the vicious cycle of inflammation within the vessel wall. However, if apoptosis occurs after establishment of the atherosclerotic plaque, more apoptosis makes the lesion more susceptible to adverse outcomes like necrosis, rupture and thrombosis. This effect is due to the inadequate efferocytosis capacity in the end-stage lesions.

Macrophages in our model show increased cholesterol uptake and decreased cholesterol efflux, which enhances their foam cell formation capacity. These macrophages also have a tendency towards pro-inflammatory phenotype (M1) and are deficient in M2 polarization. These characters are reported to be pro-atherogenic. However, we observed similar atherogenicity in MKO transplanted LDLR-/- mice. Our results indicate that increased macrophage apoptosis in the atherosclerotic lesions may be able to compensate for the pro-atherogenic and inflammatory features of IRF2BP2-deficient macrophages we observed in culture (Diagram 2).

Another possible contributor factor in atherogenesis in our mice could be the increase we saw in the HDL levels in the male IRF2BP2MKO mice after HFD feeding. Other than the central role of HDL in reverse cholesterol transport, HDL is reported to exert other functions that benefit against atherosclerosis. For instance, HDL has been shown to affect endothelial function by increasing production of endothelial Nitric oxide Synthase (eNOS), a potent vasodilator, and decreasing the expression of E-selectin, VCAM-1 and ICAM-1 which are adhesion molecules involved in leukocyte attraction (Assmann and Gotto, 2004). Moreover,

antioxidant enzymes within HDL inhibit oxidation of LDL particles and production of reactive oxygen species (Vergeer et al., 2010). On the other hand, a large genome-wide association consortium recently reported that genetic variants that strongly influence plasma HDL levels are of no consequence to the risk of coronary artery disease or associated events (Voight et al., 2012). More studies need to elucidate the origin of increased HDL in IRF2BP2MKO mice, and to investigate if this effect is present in the MKO→LDLR-/- mice.

Cardiac hypertrophy in the MKO→LDLR-/- was another intriguing outcome. It remains to be determined whether these mice have more significant aortic valve calcification, which could explain the severe septal hypertrophy in these mice. Also, Kang et al. showed that hypercholesterolemia causes cardiac hypertrophy in LDLR-/- mice fed with high cholesterol diet, and this effect is independent of blood pressure. Therefore, special features of lipid metabolism in MKO→LDLR-/- mice may have caused the cardiac muscle hypertrophy (Kang et al., 2009). This effect might also be attributed to alterations in the immune response signaling. Evidence provided by studies that showed reduction in cardiac hypertrophy in TLR4 KO mice or in mice with MyD88 blockade, support this notion (Frantz et al., 2007). Further experiments on IRF2BP2MKO mice fed with low cholesterol, high fat diet may clarify the contribution of these three possible causes.

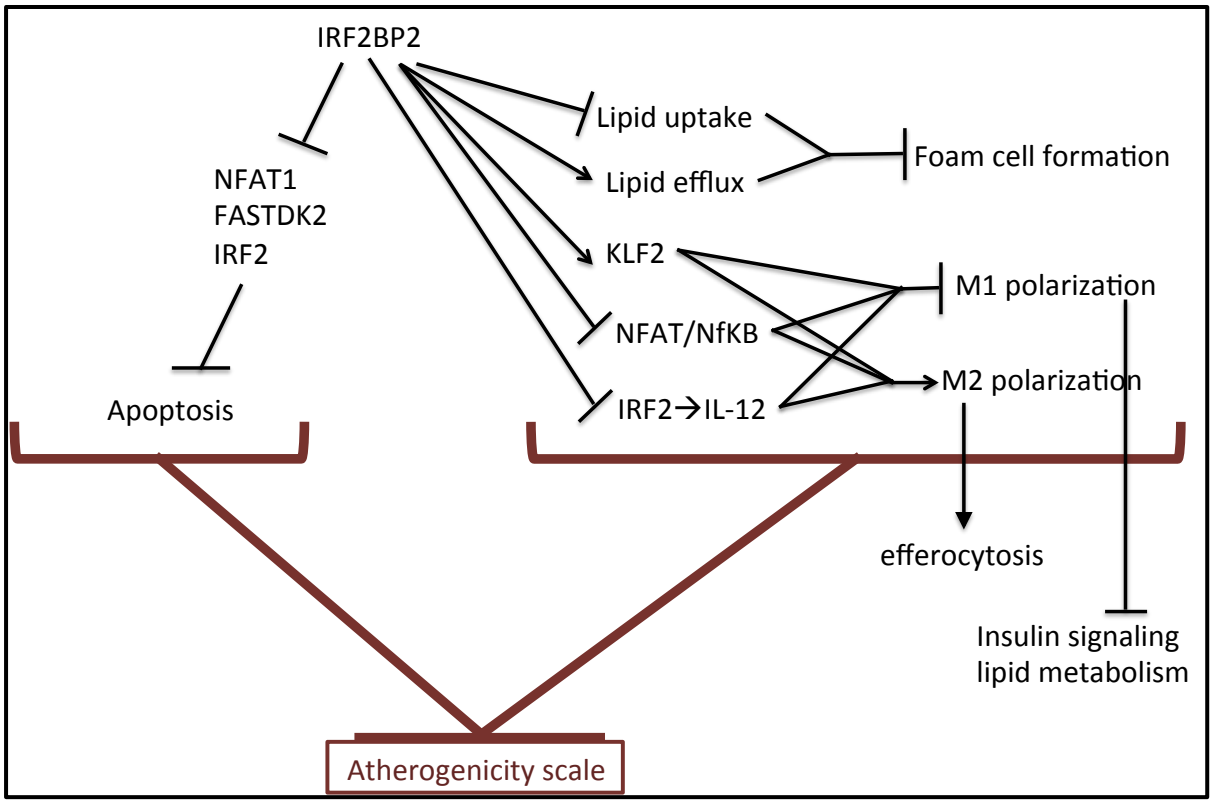

Diagram 2: Increased apoptosis in IRF2BP2-deficient macrophages balances the atherogenic inflammatory and metabolic changes in these cells.

4.4 Conclusion.

In conclusion, we demonstrated that IRF2BP2 is a key factor in normal macrophage inflammatory and metabolic function. As a result, metabolic stress on IRF2BP2MKO causes increased inflammatory state, as well as symptoms of metabolic syndrome like adiposity, glucose intolerance and hepatic steatosis. However, increased apoptosis in IRF2BP2-deficient macrophages compensates for the atherogenic inflammatory and metabolic changes in these cells, and balances the overall lesion development in IRF2BP2MKO→LDLR-/- mice. Such a phenotype has significant implications in understanding the role of macrophages in atherosclerosis process.

Chapter 5. References

Akira S, Uematsu S, Takeuchi O (2006) Pathogen recognition and innate immunity. Cell 124:783-801.

Arai S, Shelton JM, Chen M, Bradley MN, Castrillo A, Bookout AL, Mak PA, Edwards PA, Mangelsdorf DJ, Tontonoz P, Miyazaki T (2005) A role for the apoptosis inhibitory factor AIM/Spalpha/Api6 in atherosclerosis development. Cell metabolism 1:201-213.

Assmann G, Gotto AM, Jr. (2004) HDL cholesterol and protective factors in atherosclerosis. Circulation 109:III8-14.

Babaev VR, Chew JD, Ding L, Davis S, Breyer MD, Breyer RM, Oates JA, Fazio S, Linton MF (2008) Macrophage EP4 deficiency increases apoptosis and suppresses early atherosclerosis. Cell metabolism 8:492-501.

Bhargava P, Lee CH (2012) Role and function of macrophages in the metabolic syndrome. The Biochemical journal 442:253-262.

Bhasin JM, Chakrabarti E, Peng DQ, Kulkarni A, Chen X, Smith JD (2008) Sex specific gene regulation and expression QTLs in mouse macrophages from a strain intercross. PloS one 3:e1435.

Blanco JC, Contursi C, Salkowski CA, DeWitt DL, Ozato K, Vogel SN (2000) Interferon regulatory factor (IRF)-1 and IRF-2 regulate interferon gamma-dependent cyclooxygenase 2 expression. The Journal of experimental medicine 191:2131-2144.

Bojic LA, Sawyez CG, Telford DE, Edwards JY, Hegele RA, Huff MW (2012) Activation of peroxisome proliferator-activated receptor delta inhibits human macrophage foam cell formation and the inflammatory response induced by very low-density lipoprotein. Arterioscler Thromb Vasc Biol 32:2919-2928.

Boring L, Gosling J, Cleary M, Charo IF (1998) Decreased lesion formation in CCR2-/- mice reveals a role for chemokines in the initiation of atherosclerosis. Nature 394:894-897.

Brown MS, Goldstein JL (1986) A receptor-mediated pathway for cholesterol homeostasis. Science 232:34-47.

Carneiro FR, Ramalho-Oliveira R, Mognol GP, Viola JP (2011) Interferon regulatory factor 2 binding protein 2 is a new NFAT1 partner and represses its transcriptional activity. Molecular and cellular biology 31:2889-2901.

Castrillo A, Joseph SB, Vaidya SA, Haberland M, Fogelman AM, Cheng G, Tontonoz P (2003) Crosstalk between LXR and toll-like receptor signaling mediates bacterial and viral antagonism of cholesterol metabolism. Molecular cell 12:805-816.

Cavelier C, Lorenzi I, Rohrer L, von Eckardstein A (2006) Lipid efflux by the ATP-binding cassette transporters ABCA1 and ABCG1. Biochimica et biophysica acta 1761:655-666.

Charlton-Menys V, Durrington PN (2008) Human cholesterol metabolism and therapeutic molecules. Experimental physiology 93:27-42.

Chen HH, Mullett SJ, Stewart AF (2004) Vgl-4, a novel member of the vestigial-like family of transcription cofactors, regulates alpha1-adrenergic activation of gene expression in cardiac myocytes. The Journal of biological chemistry 279:30800-30806.

Childs KS, Goodbourn S (2003) Identification of novel co-repressor molecules for Interferon Regulatory Factor-2. Nucleic Acids Res 31:3016-3026.

Chinetti G, Lestavel S, Bocher V, Remaley AT, Neve B, Torra IP, Teissier E, Minnich A, Jaye M, Duverger N, Brewer HB, Fruchart JC, Clavey V, Staels B (2001) PPAR-alpha and PPAR-gamma activators induce cholesterol removal from human macrophage foam cells through stimulation of the ABCA1 pathway. Nature medicine 7:53-58.

Clausen BE, Burkhardt C, Reith W, Renkawitz R, Forster I (1999) Conditional gene targeting in macrophages and granulocytes using LysMcre mice. Transgenic research 8:265-277.

Das H, Kumar A, Lin Z, Patino WD, Hwang PM, Feinberg MW, Majumder PK, Jain MK (2006) Kruppel-like factor 2 (KLF2) regulates proinflammatory activation of monocytes. Proceedings of the National Academy of Sciences of the United States of America 103:6653-6658.

Denton FT, Spencer BG (2010) Chronic health conditions: changing prevalence in an aging population and some implications for the delivery of health care services. Canadian journal on aging = La revue canadienne du vieillissement 29:11-21.

Elser B, Lohoff M, Kock S, Giaisi M, Kirchhoff S, Krammer PH, Li-Weber M (2002) IFN-gamma represses IL-4 expression via IRF-1 and IRF-2. Immunity 17:703-712.

Fleetwood AJ, Dinh H, Cook AD, Hertzog PJ, Hamilton JA (2009) GM-CSF- and M-CSF-dependent macrophage phenotypes display differential dependence on type I interferon signaling. J Leukoc Biol 86:411-421.

Frantz S, Ertl G, Bauersachs J (2007) Mechanisms of disease: Toll-like receptors in cardiovascular disease. Nature clinical practice Cardiovascular medicine 4:444-454.

Gabelli C, Gregg RE, Zech LA, Manzato E, Brewer HB, Jr. (1986) Abnormal low density lipoprotein metabolism in apolipoprotein E deficiency. J Lipid Res 27:326-333.

Grundy SM, Brewer HB, Jr., Cleeman JI, Smith SC, Jr., Lenfant C, American Heart A, National Heart L, Blood I (2004) Definition of metabolic syndrome: Report of the National Heart, Lung, and Blood Institute/American Heart Association conference on scientific issues related to definition. Circulation 109:433-438.

Gu L, Okada Y, Clinton SK, Gerard C, Sukhova GK, Libby P, Rollins BJ (1998) Absence of monocyte chemoattractant protein-1 reduces atherosclerosis in low density lipoprotein receptor-deficient mice. Molecular cell 2:275-281.

Hanna RN, Shaked I, Hubbeling HG, Punt JA, Wu R, Herrley E, Zaugg C, Pei H, Geissmann F, Ley K, Hedrick CC (2012) NR4A1 (Nur77) deletion polarizes macrophages toward an inflammatory phenotype and increases atherosclerosis. Circulation research 110:416-427.

Hansson GK, Hermansson A (2011) The immune system in atherosclerosis. Nature immunology 12:204-212.

Hegele RA (2009) Plasma lipoproteins: genetic influences and clinical implications. Nature reviews Genetics 10:109-121.

Heger S, Mastronardi C, Dissen GA, Lomniczi A, Cabrera R, Roth CL, Jung H, Galimi F, Sippell W, Ojeda SR (2007) Enhanced at puberty 1 (EAP1) is a new transcriptional regulator of the female neuroendocrine reproductive axis. The Journal of clinical investigation 117:2145-2154.

Huang CX, Zhang YL, Wang JF, Jiang JY, Bao JL (2013) MCP-1 impacts RCT by repressing ABCA1, ABCG1, and SR-BI through PI3K/Akt posttranslational regulation in HepG2 cells. J Lipid Res 54:1231-1240.

Huang W, Metlakunta A, Dedousis N, Zhang P, Sipula I, Dube JJ, Scott DK, O'Doherty RM (2010) Depletion of liver Kupffer cells prevents the development of diet-induced hepatic steatosis and insulin resistance. Diabetes 59:347-357.

IJpenberg A, Jeannin E, Wahli W, Desvergne B (1997) Polarity and specific sequence requirements of peroxisome proliferator-activated receptor (PPAR)/retinoid X receptor heterodimer binding to DNA. A functional analysis of the malic enzyme gene PPAR response element. J Biol Chem 272:20108-20117.

Ikonen E (2008) Cellular cholesterol trafficking and compartmentalization. Nature reviews Molecular cell biology 9:125-138.

Insull W, Jr. (2009) The pathology of atherosclerosis: plaque development and plaque responses to medical treatment. The American journal of medicine 122:S3-S14.

Kanda H, Tateya S, Tamori Y, Kotani K, Hiasa K, Kitazawa R, Kitazawa S, Miyachi H, Maeda S, Egashira K, Kasuga M (2006) MCP-1 contributes to macrophage infiltration into adipose tissue, insulin resistance, and hepatic steatosis in obesity. The Journal of clinical investigation 116:1494-1505.

Kang BY, Wang W, Palade P, Sharma SG, Mehta JL (2009) Cardiac hypertrophy during hypercholesterolemia and its amelioration with rosuvastatin and amlodipine. Journal of cardiovascular pharmacology 54:327-334.

Kang K, Reilly SM, Karabacak V, Gangl MR, Fitzgerald K, Hatano B, Lee CH (2008) Adipocyte-derived Th2 cytokines and myeloid PPARdelta regulate macrophage polarization and insulin sensitivity. Cell metabolism 7:485-495.

Kansal S, Roitman D, Sheffield LT (1979) Interventricular septal thickness and left ventricular hypertrophy. An echocardiographic study. Circulation 60:1058-1065.

Kennedy MA, Barrera GC, Nakamura K, Baldan A, Tarr P, Fishbein MC, Frank J, Francone OL, Edwards PA (2005) ABCG1 has a critical role in mediating cholesterol efflux to HDL and preventing cellular lipid accumulation. Cell Metab 1:121-131.

Kimura M (2008) IRF2-binding protein-1 is a JDP2 ubiquitin ligase and an inhibitor of ATF2-dependent transcription. FEBS letters 582:2833-2837.

Koeppel M, van Heeringen SJ, Smeenk L, Navis AC, Janssen-Megens EM, Lohrum M (2009) The novel p53 target gene IRF2BP2 participates in cell survival during the p53 stress response. Nucleic acids research 37:322-335.

Kumar A, Lin Z, SenBanerjee S, Jain MK (2005) Tumor necrosis factor alpha-mediated reduction of KLF2 is due to inhibition of MEF2 by NF-kappaB and histone deacetylases. Molecular and cellular biology 25:5893-5903.

Laffitte BA, Repa JJ, Joseph SB, Wilpitz DC, Kast HR, Mangelsdorf DJ, Tontonoz P (2001) LXRs control lipid-inducible expression of the apolipoprotein E gene in macrophages and adipocytes. Proceedings of the National Academy of Sciences of the United States of America 98:507-512.

Lawn RM, Wade DP, Garvin MR, Wang X, Schwartz K, Porter JG, Seilhamer JJ, Vaughan AM, Oram JF (1999) The Tangier disease gene product ABC1 controls the cellular apolipoprotein-mediated lipid removal pathway. J Clin Invest 104:R25-31.

Lawrence T, Natoli G (2011) Transcriptional regulation of macrophage polarization: enabling diversity with identity. Nature reviews Immunology 11:750-761.

Lebedeva TV, Singh AK (1997) Constitutive activity of the murine IL-1 beta promoter is regulated by a transcriptional repressor. Biochim Biophys Acta 1353:32-38.

Lettre G et al. (2011) Genome-wide association study of coronary heart disease and its risk factors in 8,090 African Americans: the NHLBI CARe Project. PLoS Genet 7:e1001300.

Li Y, Schwabe RF, DeVries-Seimon T, Yao PM, Gerbod-Giannone MC, Tall AR, Davis RJ, Flavell R, Brenner DA, Tabas I (2005) Free cholesterol-loaded macrophages are an abundant source of tumor necrosis factor-alpha and interleukin-6: model of NF-kappaB- and map kinase-dependent inflammation in advanced atherosclerosis. The Journal of biological chemistry 280:21763-21772.

Libby P, Ridker PM, Maseri A (2002) Inflammation and atherosclerosis. Circulation 105:1135-1143.

Libby P, DiCarli M, Weissleder R (2010) The vascular biology of atherosclerosis and imaging targets. Journal of nuclear medicine : official publication, Society of Nuclear Medicine 51 Suppl 1:33S-37S.

Liu J, Thewke DP, Su YR, Linton MF, Fazio S, Sinensky MS (2005) Reduced macrophage apoptosis is associated with accelerated atherosclerosis in low-density lipoprotein receptor-null mice. Arteriosclerosis, thrombosis, and vascular biology 25:174-179.

Lopez BG, Tsai MS, Baratta JL, Longmuir KJ, Robertson RT (2011) Characterization of Kupffer cells in livers of developing mice. Comp Hepatol 10:2.

Lumeng CN, Saltiel AR (2011) Inflammatory links between obesity and metabolic disease. The Journal of clinical investigation 121:2111-2117.

Lumeng CN, Bodzin JL, Saltiel AR (2007) Obesity induces a phenotypic switch in adipose tissue macrophage polarization. The Journal of clinical investigation 117:175-184.

Maeda T, Gupta MP, Stewart AF (2002) TEF-1 and MEF2 transcription factors interact to regulate muscle-specific promoters. Biochemical and biophysical research communications 294:791-797.

Mantovani A, Garlanda C, Locati M (2009) Macrophage diversity and polarization in atherosclerosis: a question of balance. Arteriosclerosis, thrombosis, and vascular biology 29:1419-1423.

Mehta JL, Sanada N, Hu CP, Chen J, Dandapat A, Sugawara F, Satoh H, Inoue K, Kawase Y, Jishage K, Suzuki H, Takeya M, Schnackenberg L, Beger R, Hermonat PL, Thomas M, Sawamura T (2007) Deletion of LOX-1 reduces atherogenesis in LDLR knockout mice fed high cholesterol diet. Circulation research 100:1634-1642.

Miguel-Carrasco JL, Zambrano S, Blanca AJ, Mate A, Vazquez CM (2010) Captopril reduces cardiac inflammatory markers in spontaneously hypertensive rats by inactivation of NF-kB. Journal of inflammation 7:21.

Mitra S, Goyal T, Mehta JL (2011) Oxidized LDL, LOX-1 and atherosclerosis. Cardiovascular drugs and therapy / sponsored by the International Society of Cardiovascular Pharmacotherapy 25:419-429.

Moore KJ, Freeman MW (2006) Scavenger receptors in atherosclerosis: beyond lipid uptake. Arteriosclerosis, thrombosis, and vascular biology 26:1702-1711.

Moore KJ, Tabas I (2011) Macrophages in the pathogenesis of atherosclerosis. Cell 145:341-355.

Moore KJ, Sheedy FJ, Fisher EA (2013) Macrophages in atherosclerosis: a dynamic balance. Nature reviews Immunology 13:709-721.

Murray SS, Smith EN, Villarasa N, Nahey T, Lande J, Goldberg H, Shaw M, Rosenthal L, Ramza B, Alaeddini J, Han X, Damani S, Soykan O, Kowal RC, Topol EJ,

Investigators G (2012) Genome-wide association of implantable cardioverter-defibrillator activation with life-threatening arrhythmias. PLoS One 7:e25387.
Nagamoto-Combs K, Combs CK (2010) Microglial phenotype is regulated by activity of the transcription factor, NFAT (nuclear factor of activated T cells). The Journal of neuroscience : the official journal of the Society for Neuroscience 30:9641-9646.
Odegaard JI, Ricardo-Gonzalez RR, Red Eagle A, Vats D, Morel CR, Goforth MH, Subramanian V, Mukundan L, Ferrante AW, Chawla A (2008) Alternative M2 activation of Kupffer cells by PPARdelta ameliorates obesity-induced insulin resistance. Cell Metab 7:496-507.
Olefsky JM, Glass CK (2010) Macrophages, inflammation, and insulin resistance. Annual review of physiology 72:219-246.
Ouimet M, Marcel YL (2012) Regulation of lipid droplet cholesterol efflux from macrophage foam cells. Arterioscler Thromb Vasc Biol 32:575-581.
Pennings M, Meurs I, Ye D, Out R, Hoekstra M, Van Berkel TJ, Van Eck M (2006) Regulation of cholesterol homeostasis in macrophages and consequences for atherosclerotic lesion development. FEBS letters 580:5588-5596.
Prieur X, Mok CY, Velagapudi VR, Nunez V, Fuentes L, Montaner D, Ishikawa K, Camacho A, Barbarroja N, O'Rahilly S, Sethi JK, Dopazo J, Oresic M, Ricote M, Vidal-Puig A (2011) Differential lipid partitioning between adipocytes and tissue macrophages modulates macrophage lipotoxicity and M2/M1 polarization in obese mice. Diabetes 60:797-809.
Puig-Kroger A, Sierra-Filardi E, Dominguez-Soto A, Samaniego R, Corcuera MT, Gomez-Aguado F, Ratnam M, Sanchez-Mateos P, Corbi AL (2009) Folate receptor beta is expressed by tumor-associated macrophages and constitutes a marker for M2 anti-inflammatory/regulatory macrophages. Cancer Res 69:9395-9403.
Raffai RL, Hasty AH, Wang Y, Mettler SE, Sanan DA, Linton MF, Fazio S, Weisgraber KH (2003) Hepatocyte-derived ApoE is more effective than non-hepatocyte-derived ApoE in remnant lipoprotein clearance. J Biol Chem 278:11670-11675.
Reardon CA, Blachowicz L, White T, Cabana V, Wang Y, Lukens J, Bluestone J, Getz GS (2001) Effect of immune deficiency on lipoproteins and atherosclerosis in male apolipoprotein E-deficient mice. Arteriosclerosis, thrombosis, and vascular biology 21:1011-1016.
Riediger ND, Clara I (2011) Prevalence of metabolic syndrome in the Canadian adult population. CMAJ : Canadian Medical Association journal = journal de l'Association medicale canadienne 183:E1127-1134.
Rivera CA, Adegboyega P, van Rooijen N, Tagalicud A, Allman M, Wallace M (2007) Toll-like receptor-4 signaling and Kupffer cells play pivotal roles in the pathogenesis of non-alcoholic steatohepatitis. Journal of hepatology 47:571-579.
Sharif MN, Tassiulas I, Hu Y, Mecklenbrauker I, Tarakhovsky A, Ivashkiv LB (2004) IFN-alpha priming results in a gain of proinflammatory function by IL-10: implications for systemic lupus erythematosus pathogenesis. J Immunol 172:6476-6481.
Sharma N, Lu Y, Zhou G, Liao X, Kapil P, Anand P, Mahabeleshwar GH, Stamler JS, Jain MK (2012) Myeloid Kruppel-like factor 4 deficiency augments atherogenesis in ApoE-/- mice--brief report. Arterioscler Thromb Vasc Biol 32:2836-2838.
Sica A, Mantovani A (2012) Macrophage plasticity and polarization: in vivo veritas. The Journal of clinical investigation 122:787-795.

Singaraja RR, Kang MH, Vaid K, Sanders SS, Vilas GL, Arstikaitis P, Coutinho J, Drisdel RC, El-Husseini Ael D, Green WN, Berthiaume L, Hayden MR (2009) Palmitoylation of ATP-binding cassette transporter A1 is essential for its trafficking and function. Circ Res 105:138-147.

Tabas I (2005) Consequences and therapeutic implications of macrophage apoptosis in atherosclerosis: the importance of lesion stage and phagocytic efficiency. Arteriosclerosis, thrombosis, and vascular biology 25:2255-2264.

Tabas I (2010) Macrophage death and defective inflammation resolution in atherosclerosis. Nature reviews Immunology 10:36-46.

Teng AC, Al-Montashiri NA, Cheng BL, Lou P, Ozmizrak P, Chen HH, Stewart AF (2011) Identification of a phosphorylation-dependent nuclear localization motif in interferon regulatory factor 2 binding protein 2. PloS one 6:e24100.

Teng AC, Kuraitis D, Deeke SA, Ahmadi A, Dugan SG, Cheng BL, Crowson MG, Burgon PG, Suuronen EJ, Chen HH, Stewart AF (2010) IRF2BP2 is a skeletal and cardiac muscle-enriched ischemia-inducible activator of VEGFA expression. FASEB journal : official publication of the Federation of American Societies for Experimental Biology 24:4825-4834.

Teslovich TM et al. (2010) Biological, clinical and population relevance of 95 loci for blood lipids. Nature 466:707-713.

Tinnikov AA, Yeung KT, Das S, Samuels HH (2009) Identification of a novel pathway that selectively modulates apoptosis of breast cancer cells. Cancer research 69:1375-1382.

Vainio S, Ikonen E (2003) Macrophage cholesterol transport: a critical player in foam cell formation. Annals of medicine 35:146-155.

Valledor AF, Borras FE, Cullell-Young M, Celada A (1998) Transcription factors that regulate monocyte/macrophage differentiation. Journal of leukocyte biology 63:405-417.

Vergeer M, Holleboom AG, Kastelein JJ, Kuivenhoven JA (2010) The HDL hypothesis: does high-density lipoprotein protect from atherosclerosis? Journal of lipid research 51:2058-2073.

Verreck FA, de Boer T, Langenberg DM, van der Zanden L, Ottenhoff TH (2006) Phenotypic and functional profiling of human proinflammatory type-1 and anti-inflammatory type-2 macrophages in response to microbial antigens and IFN-gamma- and CD40L-mediated costimulation. J Leukoc Biol 79:285-293.

Verreck FA, de Boer T, Langenberg DM, Hoeve MA, Kramer M, Vaisberg E, Kastelein R, Kolk A, de Waal-Malefyt R, Ottenhoff TH (2004) Human IL-23-producing type 1 macrophages promote but IL-10-producing type 2 macrophages subvert immunity to (myco)bacteria. Proc Natl Acad Sci U S A 101:4560-4565.

Voight BF et al. (2012) Plasma HDL cholesterol and risk of myocardial infarction: a mendelian randomisation study. Lancet 380:572-580.

Weisberg SP, McCann D, Desai M, Rosenbaum M, Leibel RL, Ferrante AW, Jr. (2003) Obesity is associated with macrophage accumulation in adipose tissue. J Clin Invest 112:1796-1808.

White SJ, Sala-Newby GB, Newby AC (2011) Overexpression of scavenger receptor LOX-1 in endothelial cells promotes atherogenesis in the ApoE(-/-) mouse model. Cardiovascular pathology : the official journal of the Society for Cardiovascular Pathology 20:369-373.

Wilson PW, D'Agostino RB, Levy D, Belanger AM, Silbershatz H, Kannel WB (1998) Prediction of coronary heart disease using risk factor categories. Circulation 97:1837-1847.

Yan ZQ, Hansson GK (2007) Innate immunity, macrophage activation, and atherosclerosis. Immunological reviews 219:187-203.

Yeung KT, Das S, Zhang J, Lomniczi A, Ojeda SR, Xu CF, Neubert TA, Samuels HH (2011) A novel transcription complex that selectively modulates apoptosis of breast cancer cells through regulation of FASTKD2. Molecular and cellular biology 31:2287-2298.

Yue P, Chen Z, Nassir F, Bernal-Mizrachi C, Finck B, Azhar S, Abumrad NA (2010) Enhanced hepatic apoA-I secretion and peripheral efflux of cholesterol and phospholipid in CD36 null mice. PLoS One 5:e9906.